LAPPEENRANTA UNIVERSITY OF TECHNOLOGY
FACULTY OF TECHNOLOGY
DEPARTMENT OF ELECTRICAL ENGINEERING

COMBINED ELECTROMAGNETIC AND THERMAL DESIGN PLATFORM FOR TOTALLY ENCLOSED INDUCTION MACHINES

MASTER'S THESIS

Examiners: Professor Juha Pyrhönen
D.Sc. Victor Vtorov

Supervisors: Professor Juha Pyrhönen
D.Sc. Janne Nerg

Lappeenranta, May 20, 2010

Lyudmila Popova
Punkkerikatu 5 A 19
53850 Lappeenranta
lyuda-usinsk@yandex.ru

ABSTRACT

Lappeenranta University of Technology
Faculty of Technology
Department of Electrical Engineering

Lyudmila Popova

COMBINED ELECTROMAGNETIC AND THERMAL DESIGN PLATFORM FOR TOTALLY ENCLOSED INDUCTION MACHINES

Master's thesis
2010
62 pages, 25 figures, 10 tables and 1 appendix
Examiners: Professor Juha Pyrhönen, D.Sc. Victor Vtorov
Keywords: Thermal analysis, lumped-parameter thermal model, Totally Enclosed Fan Cooled (TEFC) induction machine

The aim of the thesis is to design a suitable thermal model that can be used as a tool for constructing the TEFC squirrel cage induction machine in addition to the electromagnetic model. A lumped-parameter thermal model is developed. The related problems and aspects of implementation are discussed in details. Losses are calculated analytically and the loss values are used in the thermal model. The sensitivity analysis is introduced to determine the most critical parameters of the model.

Acknowledgments

The work was carried out at Lappeenranta University of Technology during the period from winter up to spring 2010.

First of all, I would like to thank my supervisor Professor Juha Pyrhönen for useful corrections and a new knowledge obtained during my study. Special thanks to my supervisor D.Sc. Janne Nerg for great help and for his sense of humor.

I am also very grateful to Victor Vtorov for his help and participation during my study.

My deep appreciation goes to Julia Vauterin who has made my study in Lappeenranta University of Technology possible.

I would like to express my sincere gratitude to my new friends Dmitry, Polina, Sergey, Marina, Mitya, Katteden, Yulia, Pavel, Maria and to my old and the best friend Elena. Special thanks to the most wonderful and intelligent person Alexander for his support and valuable advices.
It has been a pleasure to spend this year with all of you, thanks!

Finally, I would like to express my deepest gratitude to my big family. And special thanks to my parents, my sister Elena and my brother Yury for their love and support.

Lappeenranta, May 2010
Lyudmila Popova

TABLE OF CONTENTS

List of Symbols and Abbreviations

Symbols

a	the number of parallel paths
b_{ds}	stator tooth width [m]
d_i	insulation thickness [m]
F	radial conductivity factor
F_g	geometrical factor
F_{1-2}	view factor for dissipating surface [K]
f	frequency [Hz]
G_{th}	thermal conductance
g	gravitational constant 9,81 m/s^2
$k_{Fe,n}$	correction factor
k_{sq}	skewing factor
k_w	winding factor
l	length of the stator stack [m]
l_{av}	average length of the winding turn [m]
l_b	bearing housing width [m]
l_c	total length of a conductor in a coil [m]
l_e	end-disk width [m]
l_m	distance of bearing centre to rotor mean [m]
l_0	slot winding overhang [m]
m	number of phases
$m_{Fe,n}$	mass of the magnetic circuit's section [kg]
m_s	number of stator phases
N_s	number of coil turns
Nu	Nusselt number
P	losses [W]
P_{ad}	additional losses [W]
P_{Cu}	resistive losses [W]
P_{Fe}	iron losses [W]
P_{in}	input power [W]

Pr	Prandtl number
P_{10}	losses of the material per mass unit at 1 T peak value of flux density and frequency 50 Hz [W/kg]
P_{15}	losses of the material per mass unit at 1.5 T peak value of flux density and frequency 50 Hz [W/kg]
Q_r	number of rotor bars
R	resistance [Ohm]
Ra	Rayleigh number
R_a	axial interconnecting resistance [K/W]
R_r	radial interconnecting resistance [K/W]
R_{th}	thermal resistance [K/W]
r_t	end winding toroid radius [m]
r_1	stator outer radius [m]
r_2	tooth outer radius [m]
r_3	tooth inner radius [m]
r_4	equivalent winding radius [m]
r_5	rotor outer radius [m]
r_6	end winding cross section radius [m]
r_7	end-disk inner radius [m]
r_8	equivalent rotor winding radius [m]
r_9	shaft radius [m]
S	cross-section area [m^2]
S_c	copper cross-section in slots [m^2]
S_1	contact area of endcap [m^2]
S_2	contact area of stator iron [m^2]
S_3	contact area of stator teeth [m^2]
S_4	contact area of endwinding [m^2]
S_5	contact area of rotor end-disc [m^2]
S_6	contact area of rotor iron [m^2]
s	lamination stacking factor
Ta	Taylor's number
Ta_m	modified Taylor number

T_m	mean temperature of the component [K]
β	coefficient of thermal expansion [1/K]
δ	air gap
ε	emissivity of the surface
η_f	fan efficiency
Θ	temperature rise [K]
λ	thermal conductivity of the material [W/m·K]
λ_a	aluminium conductivity [W/m·K]
λ_{air}	thermal conductivity of the air [W/m·K]
λ_c	convection coefficient [W/m^{2}K]
λ_{Cu}	copper conductivity [W/m·K]
λ_i	slot liner conductivity [W/m·K]
λ_{la}	lamination axial conductivity [W/m·K]
λ_{lr}	lamination iron conductivity [W/m·K]
λ_R	radiation heat transfer coefficient
λ_r	radial thermal conductivity [W/m·K]
λ_s	shaft steel conductivity [W/m·K]
λ_v	varnish conductivity [W/m·K]
λ_{1s}, λ_{1r}	stationary and rotating heat transfer coefficients between frame and external air [W/m^{2}K]
λ_{2s}, λ_{2r}	stationary and rotating heat transfer coefficients between stator or rotor and air gap [W/m^{2}K]
λ_{3s}, λ_{3r}	stationary and rotating heat transfer coefficients between stator iron, rotor, endwindings or endcaps and endcap air [W/m^{2}K]
μ	dynamic viscosity of the fluid [Pa s, kg/s m]
ρ	mass density of the fluid [kg/m^2]
ρ_v	transformation ratio for induction motor impedance, resistance, inductance
σ	Stefan-Boltzmann constant, $5.670400 \cdot 10^{-8}$ W/m^2/K^4

σ_c	conductivity of the conductor material [S/m]
τ_u	slot pitch [m]
υ	kinematic viscosity [Pa s/(kg/m^3)]
Φ_{th}	thermal power flow, heat flow rate [W]
ϕ_p	tooth pitch [m]
Ω	angular velocity of the rotor [rad/s]
ω	hot-spot to mean temperature ratio
ω_r	rotor angular velocity [rad/s]
ΔT	temperature rise [K, °C]

Abbreviations

CFD	computational fluid dynamics
FEM	finite-element method
IEC	International Electrotechnical Commission
PC	personal computer
TEFC	Totally Enclosed Fan-Cooled

1 INTRODUCTION

1.1 A literature review concerning thermal model of machine

In the field of a motor design, much effort is put to improve motor performance and to reduce frame size, due to increased pressure on the development of smaller, cheaper and more efficient machines. Along with the electromagnetic design, thermal design has begun to attract serious attention of design engineers. This can be explained by the fact that the temperature is the main factor, determining how long a machine can be loaded. Exceeding the thermal limits leads to various undesired phenomena: accelerated oxidation process in insulation materials, which causes the loss of dielectrical property, deterioration of bearing lubricants, mechanical stresses and changes in geometry. To predict the temperatures of a machine thermal analysis is used. The electromagnetic design and the thermal design are interrelated, it is impossible to analyze carefully one without another. As shown by Staton et al. (2005), not only the losses are dependent on the temperatures and vice-versa, but also more complex issues arise at the design stage.

Before practical computers appeared, the determination of electrical machine's sizes was made by so-called D^2L, D^3L, and D^xL sizing equations. The limiting values of specific magnetic and electric loadings and current density, obtained from previous experience were used in order to prevent overheating of the machine (Steven 1983). This method does not involve thermal analysis directly and it is not enough if a designer wants to improve motor performance, to reduce the dimensions, and vary the construction or to test new materials. In this case effective loss calculation and thermal analysis tools are required. Attempts were made to implement thermal network analysis based on lumped parameters. However, without the computer's computation capability the thermal networks were very simple, e. g., maybe just one thermal resistance to calculate the steady-state temperature rise of the winding.

The thermal network complexity could be increased considerably when introducing computers to motor design. It allowed the thermal-network analysis to be the main tool used both for steady-state and transient analysis (Mellor et al. 1991, Rajagopal et al. 1998). After the introduction of induction motor inverter supplies, the interest in thermal analysis no more involves only an electrical machine, but also the drive and power converter design (Nelson et al. 2006, Gao et al. 2008). The effect of increased losses, resulting from six-step and pulse width-modulation voltages, on motor temperatures is a subject of an intensive research (Champenois et al. 1994, Boys and Miles 1995). As a result of increased attention toward thermal analysis, the software initially used for electromagnetic design has added thermal modelling capabilities to provide better integration between the electromagnetic and thermal designs (Mezani et al. 2005, Dorrell et al. 2006, Driesen 2000, Vong and Rodger 2003).

In the thermal analysis of electrical machine analytical lumped-circuit and numerical methods are applied. The advantages of an analytical approach lie in its simple mathematical form and the high calculation speed. However, the thermal network parameters should be carefully defined to model the main heat-transfer paths (Boglietti et al. 2003, Kylander 1992, Staton 2001, Saari 1995, Saari 1998). The analysis is based on calculation of conduction, convection, and radiation resistances for different parts of the motor construction. In the lumped parameter thermal model, both radial and axial heat transfer inside the machine are considered. Also the model is able to provide transient solution (Mellor et al. 1991, Kylander 1995). An additional cooling matrix is added in the model to consider the heating of the cooling fluid (Saari 1995).

The thermal analysis tools widely use numerical methods, for example, the finite-element method (FEM) and computational fluid dynamics (CFD). Numerical analysis is very expensive in terms of a model setup and computational time. Using FEM heat conduction problems in solid components can be solved more accurately than by a thermal network. This method is well suited for solving transient problems in the machine with large temperature gradients within individual machine parts. It is a reasonable solution in machine with the main heat path in radial direction and with a low rotor speed. The drawback of FEM is that three dimensional and time-dependent problems are demanding both in software development and hardware requirements. It is also difficult to take the heating of the cooling fluid into account. The main strength of CFD approach is that it can be used to predict the flow in complex regions, such as around the motor end windings (Mgglestone et l. 1999, Staton et al. 2001). The data obtained using CFD are useful for improving the analytical model. In (Trigeol et al. 2006), a combined network and CFD method are used to model the machine. The CFD methods will be more attractive due to the increase of PC computational speed and the availability of more friendly pre- and post-processing software.

Each of the reviewed methods has advantages and disadvantages. Designers choosing one of them have to take into account the project development cost (i.e., time, result accuracy, and available resources) and the product market value.

1.2 Objectives and outline of the thesis

The present work deals with Totally Enclosed Fan-Cooled (TEFC) induction motors. These motors are probably the most commonly used motors in industrial environments. The TEFC motor has an external fan mounted opposite its drive end (Fig. 1.1). It provides additional cooling by blowing air over the motor exterior. A shroud covers the fan to prevent injury. TEFC motors can be used in dirty, moist, or mildly corrosive operating conditions, since no outside air enters the motor.

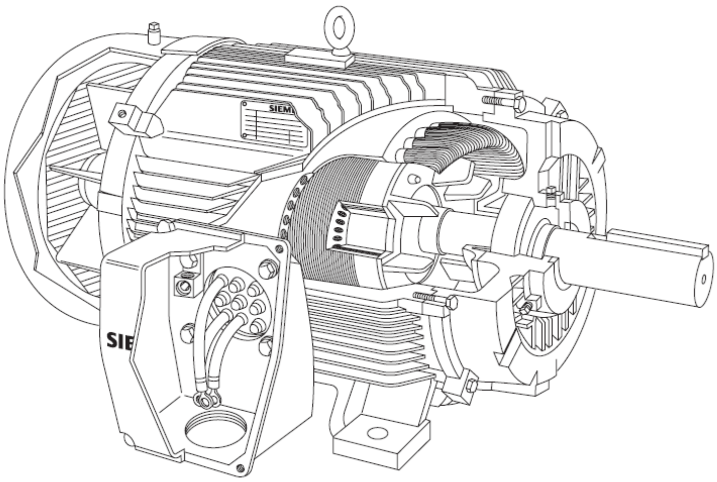

Figure 1.1 Enclosed Fan-Cooled (TEFC) induction machine (Scribd 2010)

The target is to design a suitable thermal model in addition to the electromagnetic model that can be used as a tool for constructing cage induction motors and to describe all related problems and aspects of implementation. The model is totally analytical. Losses are calculated analytically and the loss values are used in the thermal model. A thermal model that has received increased attention over the last years is a lumped parameter thermal model. This method is known to offer an adequate thermal model for low- to medium rated TEFC machines. It is not necessary to create fairy complex model for these machines, because of the basic nature of their construction and cooling. Since we have TEFC-type we do not need to model the heating of the cooling fluid. However, the model should be sufficiently detailed in order to distinguish between the stator and rotor components. Since the risk of the failure is particularly high in either the stator or rotor windings. During the thermal analysis the question of heat removal and the distribution of heat sources have to be carefully studied. In electrical machines of TEFC design heat removal is ensured by thermal convection of air, thermal conduction through the fastening of the machine, and to a less extent, by thermal radiation. The overall target is to get the knowledge of the machines steady state temperatures in the basic design stage.

2 LOSSES IN INDUCTION MOTOR

The distribution of losses in different parts of the machine is of great significance, since the heat generators that form the input to the thermal equations are derived from the motor losses. The losses in electrical machine consist of the resistive losses in stator and rotor conductors, iron losses in the magnetic circuit, additional losses and mechanical losses. The iron loss is distributed among the stator and rotor components so that the majority of the loss occurs in the components that model the stator teeth and the combined rotor bars and teeth; nodes 3 and 8.The resistive loss is divided between the slot and the end windings in proportion to the quantity of conductor in each component. The additional loss is divided in such a way that 30 percent of the loss is introduced in stator teeth, 40 percent in the windings in the slots and 30 percent in the rotor iron. The bearing losses are ignored but could be included as a heat generation in the shaft. One should keep in mind that because of symmetry only the half of the motor is considered and the half of the losses is introduced in the thermal model.

2.1 Resistive losses

The proportion of resistive losses in machine total losses is high. Resistive losses in a winding with m phases, current I and resistance R are generated according to Ohm’s law

$$P_{\mathrm{A}} = mI^2R \ . \tag{2.1}$$

Copper losses change with temperature, as resistance increase directly proportional to temperature. According to Ohm’s law the resistance R depends on the total length of a conductor in a coil l_c, the number of parallel paths a in windings without a commutator, per phase, or $2a$ in windings with a commutator, the cross-sectional area of the conductor S_c and the conductivity of the conductor material σ_c

$$R = \frac{l_c}{\sigma_c a S_c} \quad . \tag{2.2}$$

Resistance is highly dependent on the temperature of the machine. The resistance should be obtained at the highest allowable temperature for the selecting winding type. For this purpose the specific heat conductivity is found for the temperature rise Θ by the following formula

$$\sigma_c = \frac{\sigma_{c20C}}{1+\Theta\alpha_c} \quad , \tag{2.3}$$

where σ_{c20C} is the conductivity of conductor material at room temperature (+20 ºC), α_c is the temperature coefficient of resistivity for conductor. The stator windings are usually made of copper and the rotor bars are made of aluminium. The specific conductivities at room temperature and the temperature coefficients of resistivity for copper and aluminium are listed in Table 2.1.

Table 2.1 Parameters of copper and aluminium

Material	Conductivity at +20ºC/S/m	Temperature coefficient of resistivity/K
Copper	$57 \cdot 10^6$	$3.81 \cdot 10^{-3}$
Aluminium	$37 \cdot 10^6$	$3.7 \cdot 10^{-3}$

The stator resistive losses should be divided into the losses occurring in the copper in the slots and the losses in the end windings. The average length l_{av} of the winding turn of a low-voltage machine, required for losses separation is given approximately as

$$l_{av} = 2l + 2.4W + 0.1 \tag{2.4}$$

where l is the length of the stator stack, W is the average coil span.

To calculate resistive losses in the rotor the rotor resistance and rotor current referred to stator are used. When it is necessary to refer the rotor resistance to the stator, it has to be multiplied by the term (Pyrhönen et al. 2008).

$$\rho_{\mathrm{v}} = \frac{4m_{\mathrm{s}}}{Q_{\mathrm{r}}} \cdot \left(\frac{N_{\mathrm{s}} k_{\mathrm{wvv}}}{k_{\mathrm{sqvq}}} \right)^2 \tag{2.5}$$

where m_s is the number of stator phases, Q_r is the number of rotor bars, N_s is the number of coil turns, k_{wvs} is winding factor, k_{sqvr} is the skewing factor.

2.2 Iron losses

In an asynchronous machine all the parts of the machine experience an alternating flux. There are two different types of losses in an iron circuit. That are hysteresis losses and eddy current losses. If the magnetic field applied to a magnetic material is increased and then decreased back to its original value, the magnetic field inside the material does not return to its original value. The internal field 'lags' behind the external field. This behaviour results in a loss of energy, called the hysteresis loss, when a sample is repeatedly magnetized and demagnetized. Also the alternation of flux induces voltages in the conductive core material and eddy currents occur in the core. These currents resist changes in the flux. In solid objects the eddy currents considerably restrict the flux from penetrating the material. To eliminate the effect of eddy currents laminations or high-resistivity compounds are used instead of solid ferromagnetic metal cores. Also magnetic cores are made of sheet, which enables eddy currents to occur. The hysteresis losses and eddy current losses can be calculated separately, but usually manufactures give combined losses. The losses of the materials are given per mass unit at a certain peak value of flux density and frequency, for instance specific iron loss per mass for lamination material P_{15} = 6.6 W/kg, 1.5 T, 50 Hz or P_{10} = 2.09 W/kg, 1.0 T, 50 Hz.

The iron losses are obtained by dividing the magnetic circuit of the machine into n sections with approximately constant flux density. In present work the magnetic circuit is divided into the stator yoke and the stator teeth. Because of the very low fundamental frequency in the rotor, the rotor iron losses are taken into account in the additional losses.

The losses $P_{\mathrm{Fe,n}}$ of the different parts of the machine can be estimated as follows:

$$P_{\mathrm{Fe,n}} = P_{10}\left(\frac{B_{\mathrm{n}}}{1T}\right)^2 m_{\mathrm{Fe,n}} \text{ or } P_{\mathrm{Fe,n}} = P_{15}\left(\frac{B_{\mathrm{n}}}{1.5T}\right)^2 m_{\mathrm{Fe,n}}, \tag{2.6}$$

where $m_{\mathrm{Fe,n}}$ is the mass of the magnetic circuit's section.

The total losses are calculated as a sum of losses in different sections of the magnetic circuit. The problem is that the loss values P_{10} and P_{15} are valid only for a sinusoidally varying flux density. Unfortunately, the pure sinusoidal flux variation never exits in the rotating machine. There are rotating fields that have different losses compared with varying field losses. Due to field harmonics the losses will be higher. Also the stresses created in the punching of the sheet and the burrs increase the loss index. In manual calculations the iron losses can be estimated by taking into account the empirical correction coefficients $k_{\mathrm{Fe,n}}$ defined for different sections n and listed in Table 2.2 (Pyrhönen et al. 2008).

$$P_{\mathrm{Fe,n}} = \sum_{n} k_{\mathrm{Fe,n}} P_{10}\left(\frac{B_{\mathrm{n}}}{1T}\right)^2 m_{\mathrm{Fe,n}} \text{ or } P_{\mathrm{Fe,n}} = \sum_{n} k_{\mathrm{Fe,n}} P_{15}\left(\frac{B_{\mathrm{n}}}{1.5T}\right)^2 m_{\mathrm{Fe,n}}. \tag{2.7}$$

Table 2.2 Correction coefficients $k_{\mathrm{Fe,n}}$ for the definition of iron losses in different sections of different machine types taking into account above-mentioned anomalies into account.

Machine type	Teeth	Yoke
Synchronous machine	2.0	1.5-1.7
Asynchronous machine	1.8	1.5-1.7
DC machine	2.5	1.6-2.0

2.3 Additional losses

Additional losses include all the electromagnetic losses which are not taking into account in the resistive and iron losses. These losses are difficult to estimate and measure. In the IEC standards the additional losses are assumed to be 0.5 % of the input power in induction motors

$$P_{\mathrm{ad}} = 0.5 \cdot 10^{-2} P_{\mathrm{in}} \quad . \tag{2.8}$$

There are basically six mechanisms that cause additional losses in the machine (Sen and Landa 1990)

- Eddy current loss in the stator copper due to slot leakage flux
- Loss in the motor end structures due to end leakage flux
- High-frequency rotor and stator surface losses due to tooth-tip leakage flux
- Tooth pulsation and rotor copper losses due to tooth-tip leakage fluxes
- Rotor copper losses due to circulating currents induced by the leakage fluxes
- Iron losses with skewed motors due to skew-leakage flux

Additional losses are proportional to the square of the load current and to the power of 1.5 of the frequency, that is

$$P_{\mathrm{ad}} \sim I^2 f^{1.5} \tag{2.9}$$

If the additional losses are known for one pair of the current and frequency, they can be determined for another pair of current and frequency using Equation (2.9) (Pyrhönen et al. 2008).

3 THERMAL MODEL

3.1 Lumped parameter thermal model

Among different methods of thermal analysis of electrical machine, such as exact analytical calculation ('distributed loss model') and numerical analysis lumped-parameter or nodal method ('concentrated loss model') is simple but sufficiently complex to identify the temperatures at most locations in the machine. In general, the lumped parameter model is a way of simplifying the behaviour of spatially distributed systems into a topology consisting of discrete entities that approximate the behaviour of the distributed system under certain assumptions.

This method solves the thermal problems by applying thermal networks in analogy to electrical circuits, in which the mathematical analysis is much simpler than solving the Maxwell equations for the actual physical system. Table 3.1 represents the analogous thermal and electrical quantities (Pyrhönen et al. 2008).

Table 3.1 Analogous thermal and electrical quantities

Thermal flow	Symbol	Unit	Electric flow	Symbol	Unit
Quantity of heat	Q_{th}	J	Electric charge	Q	C
Heat flow rate	Φ_{th}	W	Electric current	I	A
Heat flow density	q_{th}	W/m^2	Current density	J	A/m^2
Temperature	T	K	Electric potential	V	V
Temperature rise	Θ	K	Voltage	U	V
Thermal conductivity	λ	W/m K	Electric conductivity	σ	S/m = A/V m
Thermal resistance	R_{th}	K/W	Electric resistance	R	Ω = V/A
Thermal conductance	G_{th}	W/K	Electric conductance	G	S = A/V
Heat capacity	C_{th}	J/K	Capacitance	C	F = C/V

The electrical machine is divided geometrically into a number of lumped components, each component having a heat generation and interconnections to neighbouring components through the thermal resistances. All the heat generation in the component is concentrated in one point. This point represents the *mean temperature* of the component. The lumped parameters are derived from entirely dimensional information, the thermal properties of the materials used in the design, and constant heat transfer coefficients. As a result the model is adapted to a range of frame sizes (Mellor et al. 1991). Resistive losses, iron losses, mechanical losses and additional losses represented by the heat sources, which are calculated analytically. And the thermal resistances of iron cores, windings, frame and so on are given as resistances.

The lumped parameter thermal model is allowed to include all the major components and heat transfer mechanisms within the machine. The geometry of a TEFC induction motor can be divided into the 10 components shown in Fig. 3.1, where symmetry is assumed about the shaft and a radial plane through the centre of the machine.

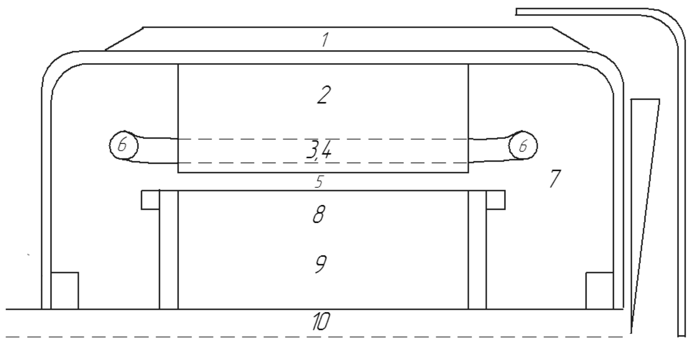

Figure 3.1 Induction motor principal construction

1 Frame	4 Stator winding	7 End cap air	10 Shaft
2 Stator iron	5 Air gap	8 Rotor winding	
3 Stator teeth	6 End winding	9 Rotor iron	

The influence of the asymmetrical temperature distribution in electrical machines is assumed to be small. The solid components of the frame (1), stator (2, 3), windings (4, 6) and rotor (8-10) have a cylindrical form so they are all modelled as a network of thermal resistances based on a general cylindrical lumped component. Two further components represent the air gap (5) and the end cap air (7). The components are connected directly or with additional thermal resistances taking into account the convective heat transfer across the cooling air paths inside the machine.

3.2 Heat transfer basics

Heat transfer is process of heat propagation. To transfer heat from one body to another the prerequisite is a temperature difference between bodies, and heat is transferred from the body with a higher temperature to a body with a lower temperature. The body with the higher temperature is called the source of heat, and the body with the lower temperature - the receiver of heat (heat sink). Methods of heat transfer are: thermal conductivity, convection and radiation.

In real conditions the heat transfer is ensured with a combined method. For example, if heat transfers between a solid wall and a gaseous medium it is transferred simultaneously by convection, conduction and radiation. Even more difficult is a process of transferring heat from a heated fluid (gas) in terms of separating their surface (heat transfer).

Usually in electrical machine of TEFC design, the most significant method of heat removal is convection through the air. However, if the motor is flange-mounted relatively large amount of heat can be removed by conduction through the flange to the device connected with the motor. The amount of heat transferred by radiation is quite small. For thermal model considered in this thesis any heat transfer due to radiation from the internal surface is neglected.

3.2.1 Conduction

When a temperature gradient exists in a body, it is known that there is energy transfer from the high-temperature region to the low temperature region. It is said that the energy is transferred by conduction and that the heat-transfer rate per unit area is proportional to the normal temperature gradient:

$$\frac{\Phi_{\mathrm{th}}}{S} \sim \frac{\partial T}{\partial x}$$

When proportionality constant is inserted,

$$\Phi_{\mathrm{th}} = -\lambda S \nabla T \text{ [W]}, \tag{3.1}$$

where Φ_{th} is the thermal power and $\partial T / \partial x$ is the temperature gradient in the direction of the heat flow. The positive constant λ is called thermal conductivity of the material, and the minus sign is inserted so that the second principle of thermodynamics will be satisfied; i.e., heat must flow downhill on the temperature scale, as indicated in the coordinate system of Fig. 3.2.

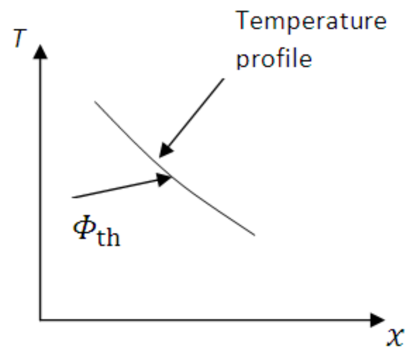

Figure 3.2 Sketch showing the direction of heat flow

Equation (3.1) is known to be Fourier's law of heat conduction and defining equation for thermal conductivity. On the basis of this definition, the thermal conductivity of different materials can be determined by experimental measurements.

Let us next consider thermal conductivities of materials used in electrical machines. Thermal energy can be transferred in solids by two modes: lattice vibration and transport by free electrons. In good electrical conductors a rather large number of free electrons move about in the lattice structure of the material. These electrons may carry thermal energy from a high-temperature region to low-temperature region as well as transport electric charge. Transmitting energy as vibrational energy in lattice structure is not as significant as the electron transport. As a result good electrical conductors are usually also good heat conductors, viz., aluminum, copper and silver. Electrical insulators are unfortunately also poor heat conductors.

Table 3.2 contains values of thermal conductivities for relevant materials in the induction machines.

Table 3.2 Conductivities of some materials

Material	Thermal conductivity λ /W/K m
Copper	400
Aluminium	237
Lamination iron	39
Shaft steel	40
Slot liner	0.3

Generally, thermal resistance R_{th} describing the conductive heat transfer in one dimension is

$$R_{\mathrm{th}} = \frac{l}{\lambda S} \ , \tag{3.2}$$

where l is the length of the body, λ is thermal conductivity and S is the cross-section area.

It is well known that the main parts of the machine are based on general cylindrical components shown in Fig. 3.3.

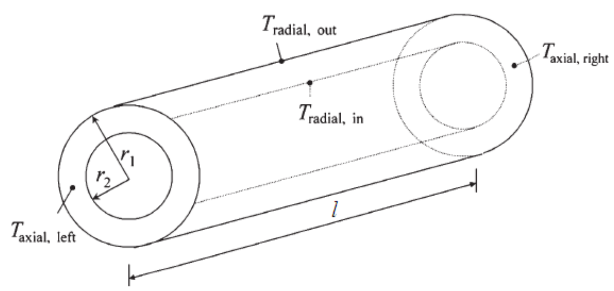

Figure 3.3 General cylindrical component with four unknown temperatures: two at the axial edges and two on the outer and inner surfaces

To describe the heat conduction across the cylindrical component, the following assumptions are maid:

- The heat flows in the radial and axial direction are independent.
- A single mean temperature defines the heat flow both in the radial and axial directions.
- There is no circumferential heat flow.
- The heat generation is uniformly distributed.

On using these assumptions, two separate three-terminal networks shown in Fig. 3.4 are obtained. One network represents the solution of the heat conduction equations in radial and axial directions.

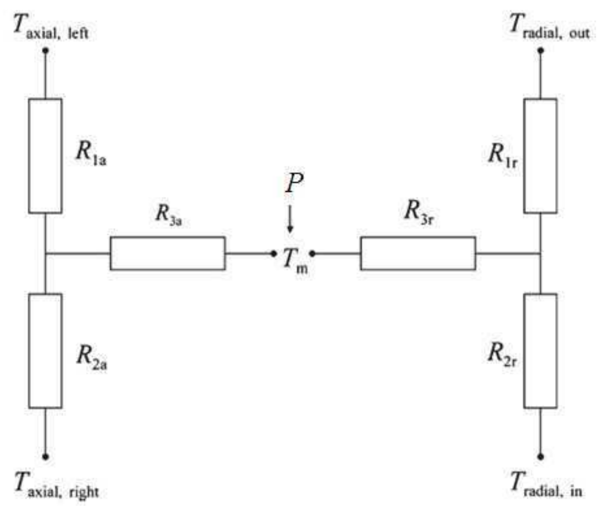

Figure 3.4 Independent axial and radial thermal networks, described by T-equivalent blocks. T_m is the average temperature, and the losses are denoted by P

In each network, two of the terminals represent the appropriate surface temperatures of the component, and the third represents the mean temperature T_m of the component. The internal heat generation is introduced in the mean temperature node. The central node of each network gives the mean temperature of the component if there is no internal heat generation. If there is heat generation the mean temperature will be obtained as a result of superposition of internal heat generation. This mean temperature is lower than the temperature given by the central node, which is reflected in the network by the negative values of the interconnecting resistances R_{3a} and R_{3r}. The thermal resistances of each network are obtained from solutions of conduction equation in the radial and axial directions. The dimensions of the cylinder and the radial and axial conductivities λ_r, λ_a are required for the calculation (Roberts 1986).

$$R_{1r} = \frac{1}{4\pi\lambda_r l} \cdot \left[1 - \frac{2r_2^2 \ln\left(\frac{r_1}{r_2}\right)}{\left(r_1^2 - r_2^2\right)} \right] \tag{3.3}$$

$$R_{2r} = \frac{1}{4\pi\lambda_r l} \cdot \left[\frac{2r_1^2 \ln\left(\frac{r_1}{r_2}\right)}{\left(r_1^2 - r_2^2\right)} - 1 \right] \tag{3.4}$$

$$R_{3r} = \frac{-1}{8\pi\left(r_1^2 - r_2^2\right)\lambda_r l} \cdot \left[r_1^2 + r_2^2 - \frac{4r_1^2 r_2^2 \ln\left(\frac{r_1}{r_2}\right)}{\left(r_1^2 - r_2^2\right)} \right] \tag{3.5}$$

$$R_{1a} = \frac{l}{2\pi\lambda_a\left(r_1^2 - r_2^2\right)} \tag{3.6}$$

$$R_{2a} = \frac{l}{2\pi\lambda_a\left(r_1^2 - r_2^2\right)} \tag{3.7}$$

$$R_{3a} = \frac{-l}{6\pi\lambda_a\left(r_1^2 - r_2^2\right)} \tag{3.8}$$

When considering conductive heat transfer in electrical machine's parts, one must keep in mind that heat conductivity can be in its maximum either in the radial or axial direction. For example, because of the presence of dielectric coating layers in laminated structures, the effective heat conductivity in the stack's axial direction is much lower than in the radial direction. And as a result the main heat transfer path is in the radial direction. In stator windings the radial heat conductivity is low, because of the presence of different insulation layers, but the axial conductivity is almost the same as for copper, ca. 400 W/m·K. The main heat transfer path is in the axial direction and the heat generated by the coil losses is removed towards the end windings, where it is removed by convection to the end cap air. Hence the maximum temperature in electrical machines is often found in the end-winding areas.

If it is assumed that the face temperatures $T_{\mathrm{axial,right}}$ and $T_{\mathrm{axial,left}}$ are equal, since the temperatures in the cylinder are symmetrical about a central radial plane. Reduced thermal network is presented in Fig. 3.5, where the half of the cylinder is modelled with only a half of heat generation.

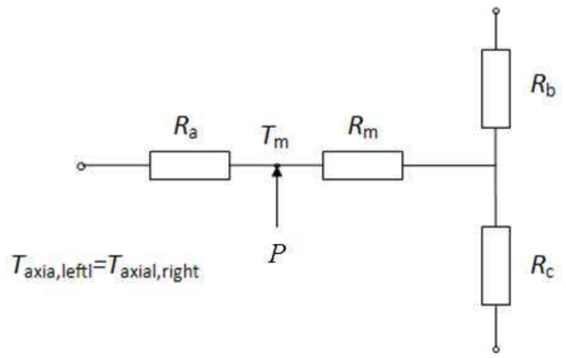

Figure 3.5 Combined thermal network for symmetric component

This network consists of two internal nodes and four thermal resistances R_a, R_b, R_c and R_m.

$$R_a = R_{1a} + R_{3a} = \frac{l}{6\pi\lambda_a\left(r_1^2 - r_2^2\right)} \tag{3.9}$$

$$R_{\mathrm{b}} = 2R_{1\mathrm{r}} = \frac{1}{2\pi\lambda_{\mathrm{r}} l} \cdot \left[1 - \frac{2r_2^2 \ln\left(\frac{r_1}{r_2}\right)}{\left(r_1^2 - r_2^2\right)} \right] \tag{3.10}$$

$$R_{\mathrm{c}} = 2R_{2\mathrm{r}} = \frac{1}{2\pi\lambda_{\mathrm{r}} l} \cdot \left[\frac{2r_1^2 \ln\left(\frac{r_1}{r_2}\right)}{\left(r_1^2 - r_2^2\right)} - 1 \right] \tag{3.11}$$

$$R_{\mathrm{m}} = 2R_{3\mathrm{r}} = \frac{-1}{4\pi\left(r_1^2 - r_2^2\right)\lambda_{\mathrm{r}} l} \cdot \left[r_1^2 + r_2^2 - \frac{4r_1^2 r_2^2 \ln\left(\frac{r_1}{r_2}\right)}{\left(r_1^2 - r_2^2\right)} \right]. \tag{3.12}$$

This combined network allows different thermal conductivities in the radial and axial directions. Thus, the thermal effect of the stator and rotor laminations can be considered.

For more detailed description of the different machine parts the axial and radial thermal resistance networks are obtained by applying (3.2) instead of T-equivalent blocks. This approach is used for modeling complex structural shapes. It allows getting desired accuracy. For example, Kylander in his work (Kylander 1995) discretized the machine by a significantly larger number of elements to obtain more information about the axial temperature distribution in the machine.

3.2.2 Convection

Convection is defined as the heat transfer between solid surfaces and a cooling fluid. Convection is a result of motion of the cooling fluid relative to the solid surface. The convective heat transfer can be modelled as a single thermal resistance

$$R_{\mathrm{th}} = \frac{1}{\lambda_c S}, \tag{3.13}$$

where S is the surface area and λ_c convection coefficient. The convection coefficient is sometimes called the film conductance because of its relation to the conduction process in the thin stationary layer of fluid at the wall surface.

In an electrical machine the convective heat transfer can be divided into external and internal. External takes place between the outside of the machine and ambient. Internal convection heat transfer is across the air gap and from the end windings to the end caps and housing.

Let us consider film coefficients used to describe the convective heat transfer from the different surfaces of induction motor. Two values of film coefficient are required for each surface. One coefficient describes stationary state of the machine, when the external and internal fans are ineffective. The second one is used for the case when machine is rotating.

These two cases are denoted by the subscripts *s* and *r*

- λ_{1s}, λ_{1r} - heat transfer between frame and external air
- λ_{2s}, λ_{2r} – heat transfer between stator or rotor via air gap
- λ_{3s}, λ_{3r} – heat transfer between stator iron, rotor, end windings or end caps and end cap air.

The coefficients λ_{1s} and λ_{1r} can be obtained directly from the test, when the motor is run at constant load until the thermal equilibrium is reached; λ_{1r} is determined from the surface-ambient temperature gradient and the total machine loss. Then, λ_{1s} is found from low-voltage locked-rotor test. Under thermal equilibrium, the heat dissipated from the motor surface is equal to the total electrical power input. It is difficult to estimate the convection from the frame to the ambient, because the frames are not the smooth cylinders. In electrical machines of TEFC design, axial fins are usually included on the housing surface to increase the convection heat transfer. A fan is fitted to the end of the shaft that blows air in the axial direction over the outside of the housing. The free convection heat transfer coefficient between frame and ambient can be estimated by Churchill-Chu equation (Churchill et al, 1972)

$$\lambda_1 = \frac{\lambda_{\mathrm{air}}}{D_{\mathrm{frame}}} \cdot \left[1.36 \cdot \frac{0.518 Ra^{1/6}}{\left(1 + \left(\frac{0.559}{\mathrm{Pr}} \right)^{9/16} \right)^{8/27}} \right]^2 , \tag{3.14}$$

where λ_{air} is the thermal conductivity of the air, D_{frame} is the frame diameter, is Ra the Rayleigh number, Pr is the Prandtl number. The equation (3.14) is valid for $10^4 \leq Ra \leq 10^9$. This number for free convection is

$$Ra = \frac{g \beta \Delta T D_{\mathrm{frame}}^3}{\upsilon^2} , \tag{3.15}$$

where g is the gravitational constant 9,81 m/s^2, β is the coefficient of thermal expansion, ΔT is the temperature difference between the surface and the fluid, υ is the fluid kinematic viscosity.

To find heat transfer coefficients between stator or rotor and air gap, the stator and the rotor are considered as two concentric cylinders rotating relative to each other. It is assumed that any heat emitted from the rotor surface is transferred directly to the stator through the air gap. The effect of heat flow from the air gap into the adjoining endcap air in axial direction is neglected. Traditionally, the air-gap film coefficients can be found in terms of a dimensionless Nusselt number Nu, the air gap width δ and the thermal conductivity of the air λ_{air}, so that

$$\lambda_2 = \frac{Nu\lambda_{\mathrm{air}}}{\delta}. \tag{3.16}$$

Becker and Kaye (Becker, K. and Kaye, J. 1962) defined Nusselt number as

$$\begin{aligned}
&Nu = 2 && \text{for } Ta_m < 1700 (\text{laminar flow}) \\
&Nu = 0.128 Ta_{\mathrm{m}}^{0.367} && \text{for } 1700 < Ta_{\mathrm{m}} < 10^4 \\
&Nu = 0.409 Ta_{\mathrm{m}}^{0.241} && \text{for } 10^4 < Ta_{\mathrm{m}} < 10^7
\end{aligned} \tag{3.17}$$

Taylor's number Ta is used to determine the flow type in the air gap. It describes the ratio of viscous forces to the centrifugal forces

$$Ta = \frac{\rho^2 \Omega^2 r \delta^3}{\mu^2}, \tag{3.18}$$

where Ω is the angular velocity of the rotor, ρ the mass density of the fluid, μ the dynamic viscosity of the fluid and r the rotor radius. The radial air gap length δ and the rotor radius are taken into account by modified Taylor number

$$Ta_{\mathrm{m}} = \frac{Ta}{F_{\mathrm{g}}}, \tag{3.19}$$

where F_{g} is the geometrical factor defined by

$$F_{\mathrm{g}} = \frac{\pi^4 \left[\frac{2r - 2.304\delta}{2r - \delta}\right]}{1697\left[0.0056 + 0.0571\left(\frac{2r - 2.304\delta}{2r - \delta}\right)^2\right]\left[1 - 2r\right]^2}. \tag{3.20}$$

In practice, F_{g} is close to unity and $Ta_{\mathrm{m}} \approx Ta$, because the air gap length is small compared with the rotor radius.

When the machine is stationary the Nusselt number is equal to 2.0, because the heat transfer across the air gap will be by conduction only.

Let us next consider film coefficient in the end cap region. It is quite a complicated task, since the heat transfer to and from all surfaces in contact with the end cap air should be considered. For simplification a single film coefficient is used to model heat transfer for each case. End cap film coefficients λ_{3s}, λ_{3r} are found from the experimental work of Luke (Luke, G. 1923), on the dissipation of heat from the end windings by forced ventilation. The film coefficient for small cooling air velocities υ can be found as

$$\lambda_{3r} = 15.5(0.29\upsilon + 1)\ \mathrm{W/m^2\ K} \tag{3.21}$$

The constant term in this expression represents the heat transfer by natural convection and is therefore the value of the stationary film coefficient λ_{3s}. The cooling air velocity can be estimated, using

$$\upsilon = r\omega_r\eta_f\,, \tag{3.22}$$

where r is the rotor radius, ω_r the rotor angular velocity and η_f is fan efficiency, which is assumed to have a rather arbitrary value of 50 %, because of the lack of available information on the radial air velocity.

The internal film coefficients for considered induction machine of TEFC design are listed in Table 3.3.

Table 3.3 Internal film coefficients of induction machine

Film coefficients	Estimated value W/m^2 K
λ_1 - film coefficient between frame and external air	15.1
λ_{2s} - stationary film coefficient between stator or rotor via air gap	65

λ_{2r} - rotating film coefficient between stator or rotor via air gap	96.9
λ_{3s} - stationary film coefficient between stator iron, rotor, end windings or end caps and end cap air	15.5
λ_{3r} - rotating film coefficient between stator iron, rotor, end windings or end caps and end cap air	83.1

The equivalent thermal resistance describes the heat transfer between two interconnected objects. In electrical machines these thermal resistances are the most significant insecurity factor. The most important thermal resistance in considered machine is the stator core to frame interface resistance, because of its position on the main heat flow path of the stator losses to the ambient. The equivalent thermal resistance can be modelled by equivalent air-gap conduction. Because of surface roughness a small air gap is assumed them. The resistance between the joint surfaces can be calculated by using Equation (3.2).The equivalent air gap length and contact heat transfer coefficients are listed in Table 3.4 (Pyrhönen et al. 2008).

Table 3.4 Equivalent joint air gap length and contact heat transfer coefficients

Joint type	Joint equivalent air gap length/mm	Contact heat transfer coefficient/W/m^2 K
Stator windings to stator core	0.10 – 0.30	80 – 250
Frame (aluminium) to stator core	0.03 – 0.04	650 – 870
Frame (cast iron) to stator core	0.05 – 0.08	350 – 550
Rotor bar to rotor core	0.01– 0.06	430 – 2600

3.2.3 Radiation

In contrast to conductive and convective heat transfer mechanisms, where heat transfers through a material medium, heat can also be transferred through regions where a perfect vacuum exists. This heat transfer mechanism is electromagnetic radiation. Thermal radiation is an electromagnetic radiation which is propagated as a result of temperature difference.

Thermal radiation is not of a great significant in electrical machines similarly as thermal convection and conduction. Radiation heat transfer is of considerable significance in the total heat transfer of an electrical machine if there is only natural convection without any fan in the system. That is why in electrical machine of TEFC design the heat transferred by radiation is often neglected. The radiation heat transfer occurs in the inner parts of the electrical machine, for instance, between the end windings and the frame, or from the frame to the surrounding medium. The amount of heat transferred by radiation depends on the temperature difference and the position between heat-exchanging surfaces.

The radiation heat transfer between surfaces can be modelled as the convective heat transfer in terms of thermal resistances, which can be simply calculated for a given surface using

$$R_{\mathrm{th}} = \frac{1}{\lambda_{\mathrm{R}} S}, \tag{3.21}$$

where S (in square meters) is the surface area and λ_{R} (in watt per square meter degree Celsius) is the radiation heat transfer coefficient. The surface area is easily calculated from the surface geometry. The radiation heat transfer coefficient can be calculated using

$$\lambda_R = \sigma \varepsilon F_{1-2} \frac{\left(T_1^4 - T_2^4\right)}{\left(T_1 - T_2\right)}, \tag{3.22}$$

where σ is the Stefan-Boltzmann constant, ε is the emissivity of the surface, $F_{1\text{-}2}$ is the view factor for dissipating surface 1 to absorbing surface 2, and T_1 and T_2 are the temperatures of surfaces 1 and 2 (in Kelvin). The emissivity is a function of the surface material and finish, for which the data can be found in the most of engineering textbooks. The emissivities of some materials in typical electrical machines are listed in Table 3.5 (Pyrhönen et al. 2008).

Table 3.5 Emissivities of some material used in electrical machines

Material	Emissivity
Polished aluminium	0.04
Polished copper	0.025
Mild steel	0.2 – 0.3
Cast iron	0.3
Stainless steel	0.5 – 0.6
Black paint	0.9 – 0.95
Aluminium paint	0.5

It is easy to calculate the view factor for simple geometric surfaces, such as cylinders and flat plates, but it can be more difficult for complex geometries, such as open-fin channels. In (Modest 2003) and (Rea et al. 1976) the methods for the view factor calculation are presented.

3.3 Computation of nodal temperatures

The target of this work is to find mean temperatures of thermal model elements. The thermal model of TEFC induction model consists of 10 nodes and is presented in Fig. 3.6.

The machine elements are represented by the temperature rise, which is the temperature difference between the element and the ambient air temperature.

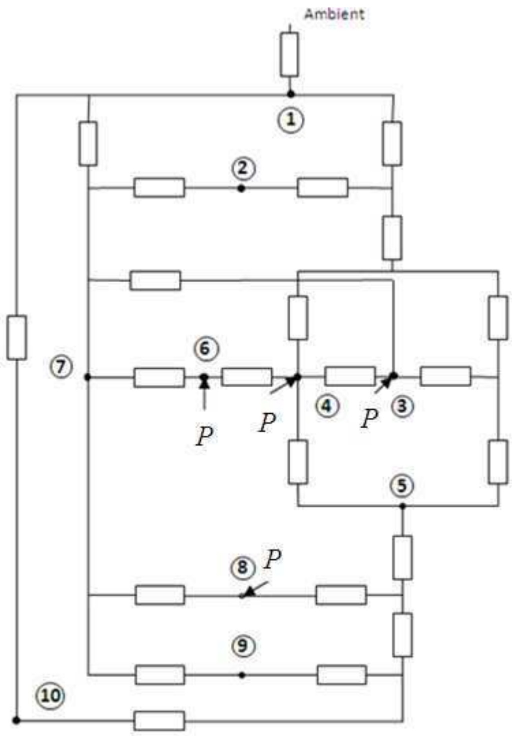

Figure 3.6 Total induction motor thermal network

P – nodal heat generation

1 Frame	4 Stator winding	7 End cap air	10 Shaft
2 Stator iron	5 Air gap	8 Rotor winding	
3 Stator teeth	6 End winding	9 Rotor iron	

For steady-state analysis, the temperature rise for each node is calculated with the matrix equation

$$\Delta\mathbf{T} = \mathbf{G}^{-1}\mathbf{P}\,, \tag{3.23}$$

where **P** is vector containing the losses in each node, $\Delta\mathbf{T}$ is the temperature rise vector. The resistances of thermal network elements are used to obtain a $n \times n$ thermal conductance matrix **G**, where n is a number of nodes in the model. A conductance matrix is defined as

$$\mathbf{G} = \begin{bmatrix} \sum_{i=1}^{n} \frac{1}{R_{1,i}} & -\frac{1}{R_{1,2}} & \cdots & -\frac{1}{R_{1,n}} \\ -\frac{1}{R_{2,1}} & \sum_{i=1}^{n} \frac{1}{R_{2,i}} & \cdots & -\frac{1}{R_{2,n}} \\ \vdots & \vdots & \ddots & \vdots \\ -\frac{1}{R_{n,1}} & -\frac{1}{R_{n,2}} & \cdots & \sum_{i=1}^{n} \frac{1}{R_{n,1}} \end{bmatrix}, \tag{3.24}$$

where the *n*th diagonal element is the sum of the network conductances connected to the node *n*, *G(i,j)* is the thermal conductance connected the nodes *i* and *j* with a minus sign (Nerg et al. Oct. 2008).

Steady-state solution is obtained from Eq. (3.23), but some of the parameters in **G** and **P** are temperature-dependent, so an iterative process should be used where the temperature-dependent parameters are updated until the error is sufficiently small.

4 DETAILS OF MOTOR COMPONENTS

The present chapter gives details of the geometries and formulas for each of the ten networks of thermal resistances. These networks are combined to form the total mesh for the entire machine presented in Fig. 4.1 and the explanations of different thermal resistances are listed in Table 4.1.

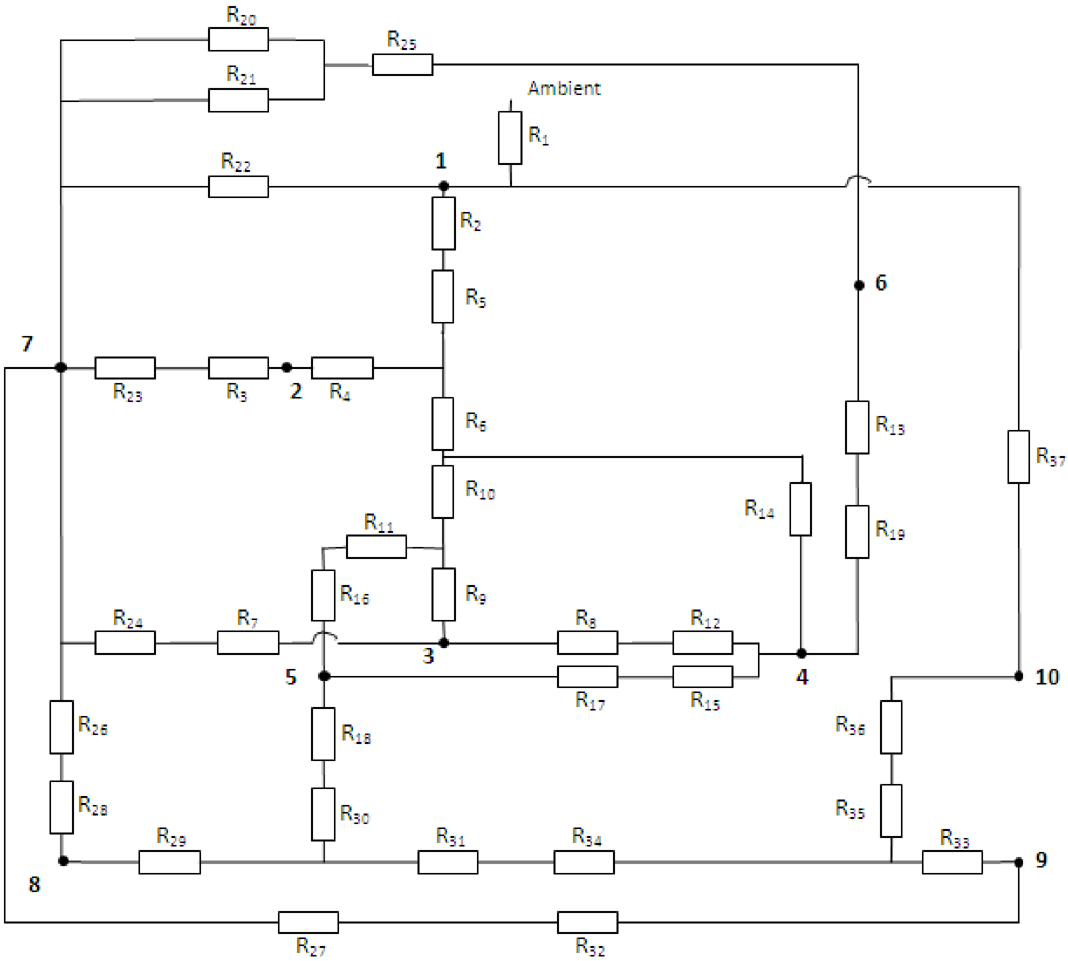

Figure 4.1 Total induction motor thermal network

Table 4.1 Thermal resistances and their explanations of the network

Component	Explanation
R_1	Thermal resistance from frame to ambient
R_2	Radial thermal resistance from frame to stator yoke
R_3	Axial thermal resistance from stator yoke to end cap air
R_4	Radial interconnecting thermal resistance of the stator yoke
R_5	Radial thermal resistance from the stator yoke to frame

R_6	Radial thermal resistance from the stator yoke to stator teeth
R_7	Axial thermal resistance from stator teeth to end cap air
R_8	Radial/circumferential thermal resistance from stator teeth to stator
R_9	Radial interconnecting thermal resistance of the stator teeth
R_{10}	Radial thermal resistance from the stator teeth to stator yoke
R_{11}	Radial thermal resistance from the stator teeth to air gap
R_{12}	Radial/circumferential thermal resistance from the stator coils to stator
R_{13}	Axial thermal resistance from the stator coils to end-winding
R_{14}	Radial thermal resistance from the stator coils to stator yoke
R_{15}	Radial thermal resistance from the stator coils to air gap
R_{16}	Radial thermal resistance from the air gap to stator teeth
R_{17}	Radial thermal resistance from the air gap to stator coils
R_{18}	Radial thermal resistance from the air gap to rotor bars
R_{19}	Axial thermal resistance from the end-winding to stator coils
R_{20}	Thermal resistance from the end-winding to end cap air
R_{21}	Thermal resistance from the end-winding to end cap air
R_{22}	Axial thermal resistance from the end cap air to frame
R_{23}	Axial thermal resistance from the end cap air to stator yoke
R_{24}	Thermal resistance from the end cap air to stator teeth
R_{25}	Thermal resistance from the end cap air to end-winding
R_{26}	Thermal resistance from the end cap air to rotor end-rings
R_{27}	Thermal resistance from the end cap air to rotor iron
R_{28}	Axial thermal resistance from the rotor bars to end cap air
R_{29}	Radial interconnecting thermal resistance of the rotor bars
R_{30}	Radial thermal resistance from the rotor bars to air gap
R_{31}	Radial thermal resistance from the rotor bars to rotor iron
R_{32}	Axial thermal resistance from the rotor iron to end cap air
R_{33}	Radial interconnecting thermal resistance of the rotor iron
R_{34}	Radial thermal resistance from the rotor iron to rotor bars
R_{35}	Radial thermal resistance from the rotor iron to shaft
R_{36}	Radial thermal resistance from the shaft to rotor iron
R_{37}	Axial thermal resistance from the shaft to frame through bearings

Only half of the machine is observed due to symmetry about the shaft and a radial plane through the centre of the machine. Simplifications and assumptions made in applying the conduction and convection models to the networks of each component are given below.

4.1 Frame

The frame component consists of the entire ribbed cooling structure and the end caps (Fig. 4.2).

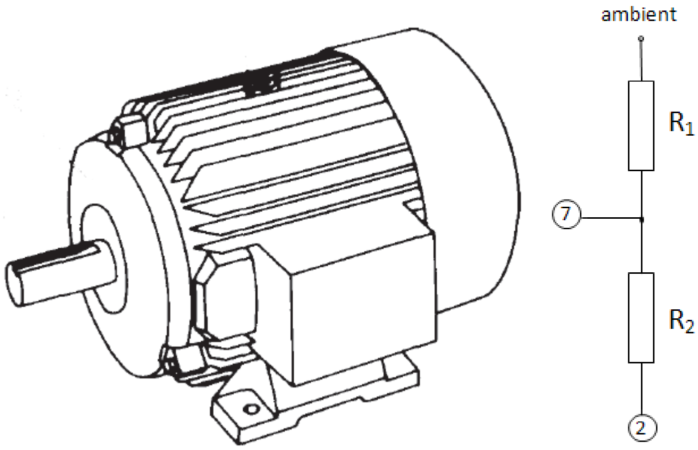

Figure 4.2 Frame

The frame is assumed to dissipate the heat by convection and radiation through a single frame to ambient thermal resistance R_1.

$$R_1 = \frac{1}{\lambda_1 S_{\text{frame}}}, \tag{4.1}$$

where λ_1 is the free convection heat transfer coefficient between frame and ambient and S_{frame} is the half of frame area. The radiation coefficient is equal to the free convection coefficient. The surface area is increased by 50 % to take into account the housing fins.

The heat is received from the stator across the frame-core contact resistance and from the end cap air by convection.

$$R_2 = \frac{1}{\pi \lambda_{\text{cont}} l r_1}, \tag{4.2}$$

where l is stator length, λ_{cont} is frame-core contact coefficient, r_1 is stator outer radius.

4.2 Stator iron

The stator back iron component contains the stator lamination minus the stator teeth. The general cylinder form is modified to account for anisotropy due to the laminations. A stacking factor in the radial direction is introduced and a value lower than that of mild steel for the axial conductivity obtained from data given by General Electric (1969) is used.

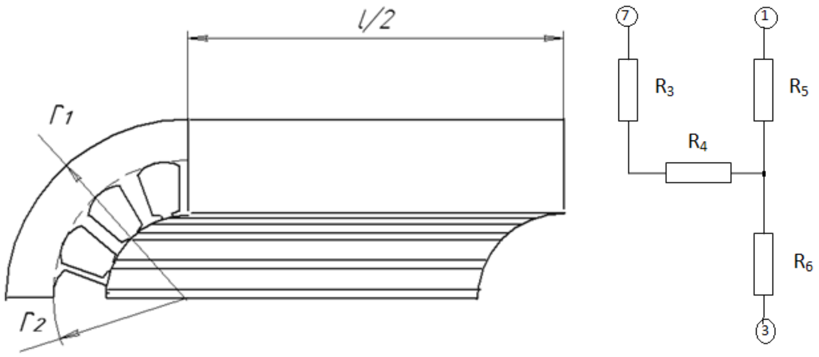

Figure 4.3 Stator iron

$$R_3 = \frac{l}{6\pi\lambda_{la}\left(r_1^2 - r_2^2\right)} \tag{4.3}$$

$$R_4 = \frac{-1}{4\pi\lambda_{lr} ls\left(r_1^2 - r_2^2\right)} \cdot \left[r_1^2 + r_2^2 - \frac{4r_1^2 r_2^2 \ln\left(\frac{r_1}{r_2}\right)}{r_1^2 - r_2^2} \right] \tag{4.4}$$

$$R_5 = \frac{1}{2\pi\lambda_{lr} ls} \cdot \left[1 - \frac{2r_2^2 \ln\left(\frac{r_1}{r_2}\right)}{r_1^2 - r_2^2} \right] \tag{4.5}$$

$$R_6 = \frac{1}{2\pi\lambda_{lr} ls} \cdot \left[\frac{2r_1^2 \ln\left(\frac{r_1}{r_2}\right)}{r_1^2 - r_2^2} - 1 \right] \tag{4.6}$$

Here λ_{la} is lamination axial conductivity, λ_{lr} is lamination iron conductivity, r_1 is stator outer radius, r_2 is tooth outer radius.

4.3 Stator teeth

The stator teeth are modelled as a collection of cylindrical segments connected thermally in parallel. The stator tooth width b_{ds} is calculated to give a segment cross-sectional area equal to that of the actual tooth profile. Additional resistance between the slot faces to the point of mean temperature at the tooth is used to model the circumferential heat flow from slot windings to the point of mean temperature. The assumptions for the lamination are made as for the stator back iron.

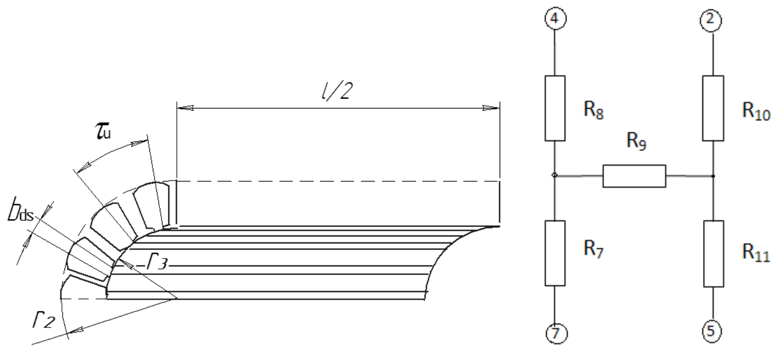

Figure 4.4 Stator teeth

$$R_7 = \frac{l\tau_u}{6\pi\lambda_{la} b_{ds}\left(r_2^2 - r_3^2\right)} \tag{4.7}$$

$$R_8 = \frac{\pi b_{ds}\left(r_2^2 - r_3^2\right)}{\lambda_{lr} ls\tau_u\left(r_2^2 - r_3^2\right)^2 n^2} \tag{4.8}$$

$$R_9 = \frac{-1}{4\pi\lambda_{\mathrm{lr}} l s b_{\mathrm{ds}} \left(r_2^2 - r_3^2\right)} \cdot \left[r_2^2 + r_3^2 - \frac{4 r_2^2 r_3^2 \ln\left(\frac{r_2}{r_3}\right)}{r_2^2 - r_3^2} \right] \qquad (4.9)$$

$$R_{10} = \frac{\tau_{\mathrm{u}}}{2\pi\lambda_{\mathrm{lr}} l s b_{\mathrm{ds}}} \cdot \left[1 - \frac{2 r_3^2 \ln\left(\frac{r_2}{r_3}\right)}{r_2^2 - r_3^2} \right] \qquad (4.10)$$

$$R_{11} = \frac{\tau_{\mathrm{u}}}{2\pi\lambda_{\mathrm{lr}} l s b_{\mathrm{ds}}} \cdot \left[\frac{2 r_2^2 \ln\left(\frac{r_2}{r_3}\right)}{r_2^2 - r_3^2} - 1 \right]. \qquad (4.11)$$

Here r_3 is tooth inner radius, τ_{u} is tooth pitch, b_{ds} is stator tooth width, n is number of slots and s is lamination stacking factor.

4.4 Stator winding

The stator windings that lie in the slots are modelled as solid cylindrical rods consisted of an array of conductors and insulation. The copper conductors are assumed to transfer the heat axially along the slot, but radially the winding is considered as a homogeneous solid which has a conductivity that is 2.5 times that of the insulation alone (General Electric, 1969). ‘The radius of the rod is chosen to give a cross-section equivalent to that of the available area in the slot assuming a 100 % slot fill’ (Mellor et al. 1991). The slot liner is modelled separately as a polyamide strip of thickness consistent with the class of insulation used in the machine.

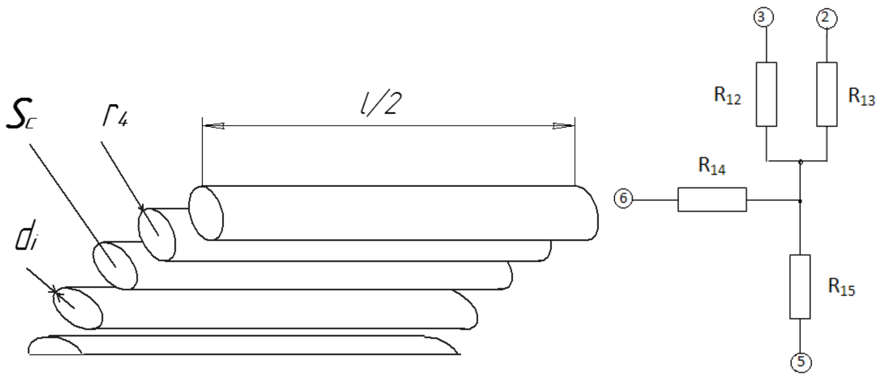

Figure 4.5 Stator winding

$$R_{12} = \frac{2d_{\mathrm{i}}}{\pi \lambda_{\mathrm{i}} l r_4 n} + \frac{1}{2\pi \lambda_{\mathrm{v}} l F n} \tag{4.12}$$

$$R_{13} = \frac{l}{6\lambda_{\mathrm{Cu}} S_{\mathrm{c}} n} \tag{4.13}$$

$$R_{14} = \frac{4d_{\mathrm{i}}}{\pi \lambda_{\mathrm{i}} l r_4 n} + \frac{1}{\pi \lambda_{\mathrm{v}} l F n} \tag{4.14}$$

$$R_{15} = \frac{1}{\pi \lambda_{\mathrm{v}} l F n}\,. \tag{4.15}$$

Here r_4 is equivalent winding radius, d_{i} is insulation thickness, S_{c} is copper cross-section in slots, F is radial conductivity factor, λ_{Cu} is copper conductivity, λ_{i} is slot liner conductivity and λ_{v} is varnish conductivity.

4.5 Air gap

The air gap forms a connection between the stator teeth, the part of the stator winding exposed in the slot opening and the rotor surface. To calculate the thermal resistances the contact areas of these solids and air-gap film coefficients are found.

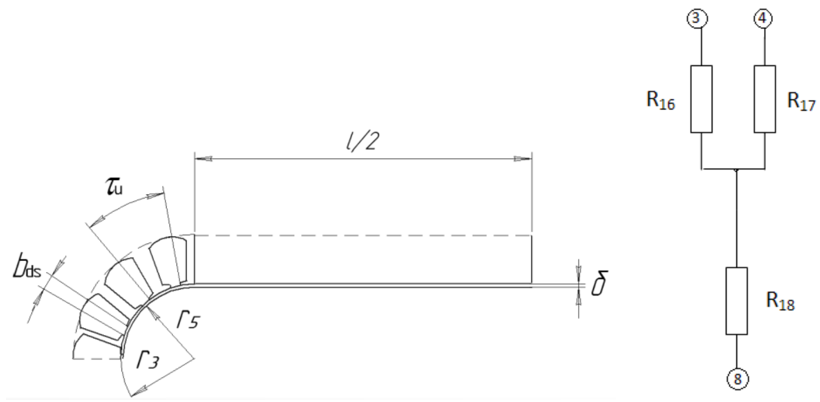

Figure 4.6 Air gap

$$R_{16} = \frac{\tau_{\mathrm{u}}}{b_{\mathrm{ds}} \pi r_3 l \lambda_{2\mathrm{r}} [\lambda_{2\mathrm{s}}]} \tag{4.16}$$

$$R_{17} = \frac{\tau_{\mathrm{u}}}{(\tau_{\mathrm{u}} - b_{\mathrm{ds}}) \pi r_3 l \lambda_{2\mathrm{r}} [\lambda_{2\mathrm{s}}]} \tag{4.17}$$

$$R_{18} = \frac{1}{\pi r_5 l \lambda_{2\mathrm{r}} [\lambda_{2\mathrm{s}}]} . \tag{4.18}$$

Here r_5 is rotor outer radius, λ_{2r} is rotating air-gap film coefficient, λ_{2s} is stationary air-gap film coefficient.

4.6 End winding

The end winding is considered as a homogeneous structure, consisting of conductors and insulation. The legs are short cylindrical extensions of the stator slot windings. As in the slot winding, the radial heat is assumed to be that of homogeneous rods. In the axial direction heat transfer occurs from the mean temperature point in the toroid to the stator slot winding along the copper conductors of the legs. The external toroid radius is considered as the mean radius of the stator slots.

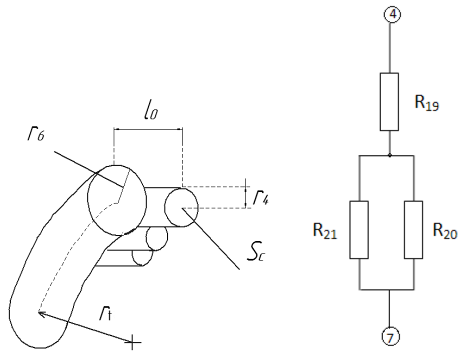

Figure 4.7 End winding

The peak hot-spot temperature in the end winding is more important than the mean temperature. It is of great importance in the evaluation of insulation aging and failure. A ratio of peak to mean temperatures of 1.5:1 is obtained from the theoretical solution of the heat conduction equation. This factor is used to obtain the peak temperature by weighting the thermal resistances of the end winding model.

$$R_{19} = \frac{l_0 \omega}{n S_c \lambda_{Cu}} \tag{4.19}$$

$$R_{20} = \frac{\omega}{16\pi^2 r_t F \lambda_v} \tag{4.20}$$

$$R_{21} = \frac{\omega r_6^2}{8\pi r_4^2 l_0 F \lambda_v n} . \tag{4.21}$$

Here r_t is endwinding toroid radius, r_6 is endwinding cross section radius, l_0 is slot winding overhang, ω is hot-spot to mean temperature ratio.

4.7 End cap air

The temperature of the circulating air in the end cap is assumed to be uniform. A single film coefficient describes the convective heat transfer from all surfaces.

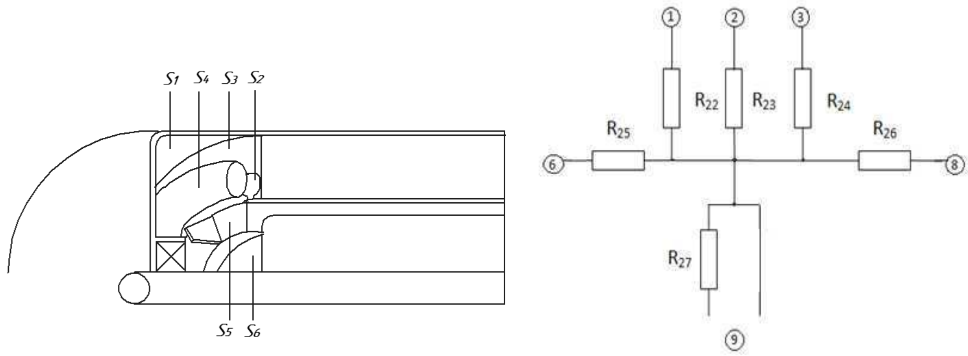

Figure 4.8 End cap air

The contact area of the endwinding toroidal model is increased by 50% to allow for surface irregularities and the greater area of the flatter structure of a true endwinding.

$$R_{22} = \frac{1}{S_1 \lambda_{3r}[\lambda_{3s}]} \tag{4.22}$$

$$R_{23} = \frac{1}{S_2 \lambda_{3r}[\lambda_{3s}]} \tag{4.23}$$

$$R_{24} = \frac{1}{S_3 \lambda_{3r}[\lambda_{3s}]} \tag{4.24}$$

$$R_{25} = \frac{1}{1.5 S_4 \lambda_{3r}[\lambda_{3s}]} \tag{4.25}$$

$$R_{26} = \frac{1}{S_5 \lambda_{3r}[\lambda_{3s}]} \tag{4.26}$$

$$R_{27} = \frac{1}{S_6 \lambda_{3r}[\lambda_{3s}]}. \tag{4.27}$$

Here S_1 is contact area of end cap, S_2 is contact area of stator iron, S_3 is contact area of stator teeth, S_4 is contact area of end winding, S_5 is contact area of rotor end-disc, S_6 is contact area of rotor iron, λ_{3r} is rotating end cap film coefficient, λ_{3s} is stationary end cap film coefficient.

4.8 Rotor winding

The rotor winding is modelled as a continuous aluminium cylinder surrounding the rotor core, which has a volume equal to that of the cage bars. Joined to the end of the winding is a disc of equivalent volume to the total end-disc including the fan. The assumptions are reasonable because a good contact exists between the extruded aluminium bars and the rotor laminations.

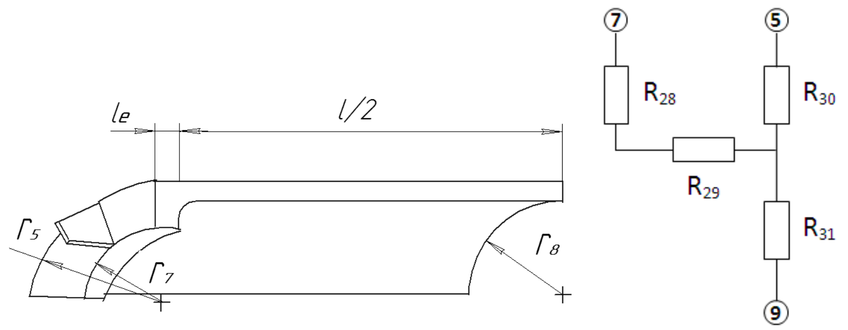

Figure 4.9 Rotor winding

$$R_{28} = \frac{l}{6\pi\lambda_a\left(r_5^2 - r_8^2\right)} + \frac{l_e}{\pi\lambda_a\left(r_5^2 - r_7^2\right)} \tag{4.28}$$

$$R_{29} = \frac{-1}{4\pi\lambda_a l\left(r_5^2 - r_8^2\right)} \cdot \left[r_5^2 + r_8^2 - \frac{4r_5^2 r_8^2 \ln\left(\frac{r_5}{r_8}\right)}{r_5^2 - r_8^2} \right] \tag{4.29}$$

$$R_{30} = \frac{1}{2\pi\lambda_a l} \cdot \left[1 - \frac{2r_8^2 \ln\left(\frac{r_5}{r_8}\right)}{r_5^2 - r_8^2} \right] \tag{4.30}$$

$$R_{31} = \frac{1}{2\pi\lambda_{\mathrm{a}} l} \cdot \left[\frac{2r_5^2 \ln\left(\frac{r_5}{r_8}\right)}{r_5^2 - r_8^2} - 1 \right]. \tag{4.31}$$

Here r_7 is end-disk inner radius, r_8 is equivalent rotor winding radius, l_{e} is end-disk width, λ_{a} is aluminium conductivity.

4.9 Rotor iron

The assumptions for taking into account lamination are the same as for stator iron.

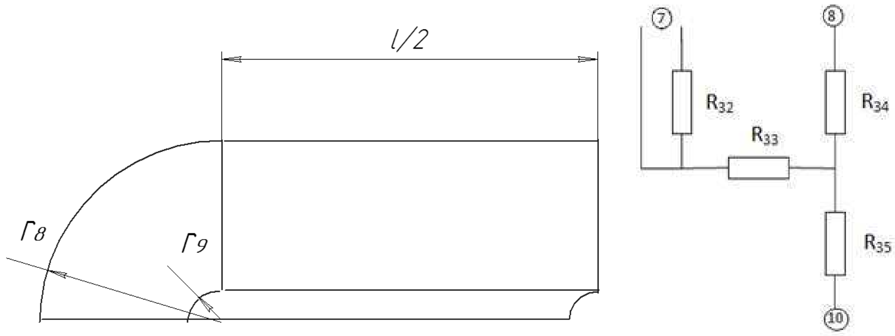

Figure 4.10 Rotor iron

$$R_{32} = \frac{l}{6\pi\lambda_{1\mathrm{a}}\left(r_8^2 - r_9^2\right)} \tag{4.32}$$

$$R_{33} = \frac{-1}{4\pi\lambda_{1\mathrm{r}} ls\left(r_8^2 - r_9^2\right)} \cdot \left[r_8^2 + r_9^2 - \frac{4r_8^2 r_9^2 \ln\left(\frac{r_8}{r_9}\right)}{r_8^2 - r_9^2} \right] \tag{4.33}$$

$$R_{34} = \frac{r_8^2 - r_9^2}{2\pi\lambda_{1\mathrm{r}} ls\left(r_8^2 - r_9^2\right)} \cdot \left[1 - \frac{2r_9^2 \ln\left(\frac{r_8}{r_9}\right)}{r_8^2 - r_9^2} \right] \tag{4.34}$$

$$R_{35} = \frac{r_8^2 - r_9^2}{2\pi\lambda_{\mathrm{lr}} ls\left(r_8^2 - r_9^2\right)} \cdot \left[\frac{2r_8^2 \ln\left(\dfrac{r_8}{r_9}\right)}{r_8^2 - r_9^2} - 1 \right]. \tag{4.35}$$

Here r_9 is shaft radius.

4.10 Shaft

The shaft is modelled as a cylindrical rod without heat generation. Three sections are used to model the axial heat conduction. One section is under the rotor iron, the second is under bearings and the third is a thermal connection between the mean temperatures of the first two. Temperature at the centre of the third section is the mean temperature of the entire shaft. It is assumed to be a good thermal contact between the shaft and the frame across the bearings. Any shaft external to the bearings is treated as a part of the frame.

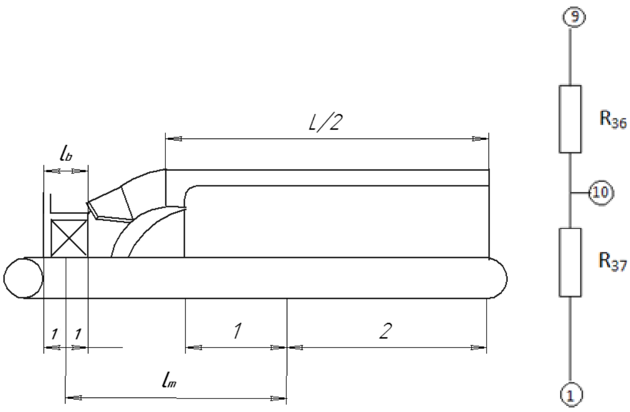

Figure 4.11 Shaft

$$R_{36} = \frac{1}{2\pi\lambda_{\mathrm{s}} l} + \frac{l_{\mathrm{m}}}{2\pi\lambda_{\mathrm{s}} r_9^2} \tag{4.36}$$

$$R_{37} = \frac{1}{4\pi\lambda_{\mathrm{s}} l_{\mathrm{b}}} + \frac{l_{\mathrm{m}}}{2\pi\lambda_{\mathrm{s}} r_9^2}. \tag{4.37}$$

Here l_b is bearing housing width, l_m is distance of the bearing centre to rotor mean and λ_s is shaft steel conductivity.

5 STEADY-STATE ANALYSIS

The calculation sheet was developed for the steady-state solution of the thermal network. The dimensions, rotation speed, electromagnetic losses of the machine were calculated during analytical electromagnetic design. These data as cooling method, material properties and thermal conductivities are given as input values (Table 5.1). The convection heat-transfer coefficients are found by equations presented in Section 3.2.2. Chapter 4 is dedicated to introduce the calculation of thermal resistances of the machine parts.

Table 5.1 Initial data of a three-phase squirrel cage induction motor with a two-layer integral slot winding and totally enclosed fan cooling

Rated power, W	$P = 30 \cdot 10^3$
Synchronous speed, 1/min	$n_{syn} = 1500$
Line-to-line voltage star connected, V	$U = 690$
Phase voltage, V	$U_{sph} = \frac{U}{\sqrt{3}}$ $U_{sph} = 398.3717$
Number of phases	$m = 3$
Number of pole pairs	$p = 2$
Frequency, Hz	$f = \frac{n_{syn}}{60} \cdot p$ $f = 50$
Stator angular frequency, rad/s	$\omega = 2 \cdot \pi \cdot f$ $\omega = 314.1593$
Rated power factor, estimated	$\cos\varphi_n = 0.84$
Rated efficiency, estimated	$\eta = 0.927$
Permeability of vacuum, VsA-1m-1	$\mu_0 = 4 \cdot \pi \cdot 10^{-7}$
Temperature rise in the windings, K	$\Theta = 80$
Conductivity of copper at 20 degrees C, S/m	$\sigma_{Cu20C} = 57 \cdot 10^6$
Temperature coefficient of copper	$\alpha_{Cu} = 3.81 \cdot 10^{-3}$
Density of copper, kg/m3	$\rho_{Cu} = 8960$
Conductivity of aluminium at 20 degrees C, S/m	$\sigma_{Al20C} = 37 \cdot 10^6$
Temperature coefficient of aluminium	$\alpha_{Al} = 3.7 \cdot 10^{-3}$
Density of aluminium, kg/m3	$\rho_{Al} = 2700$

Space factor of stator and rotor core	$k_{\mathrm{Fe}} = 0.97$
Density of iron, kg/m3	$\rho_{\mathrm{Fe}} = 7600$
The specific iron loss per mass at 1.5 T and 50 Hz with M800-50 A, W/kg	$P_{15} = 6.6$
Enclosure type	IP 55,dust proof, water tolerant
Duty type	S1
Cooling method	surface-cooled IC 41 with an external fan attached on the motor shaft
Thermal class	155 (F)

5.1 Calculation results

The thermal network is obtained by the method described in Section 3.3. For steady-state analysis the temperature rise vector is obtained by the Eq. 3.23. The temperature of 40 ℃ is chosen as a reference temperature. The calculated temperatures of the different parts of the machine are presented in the Fig. 5.1.

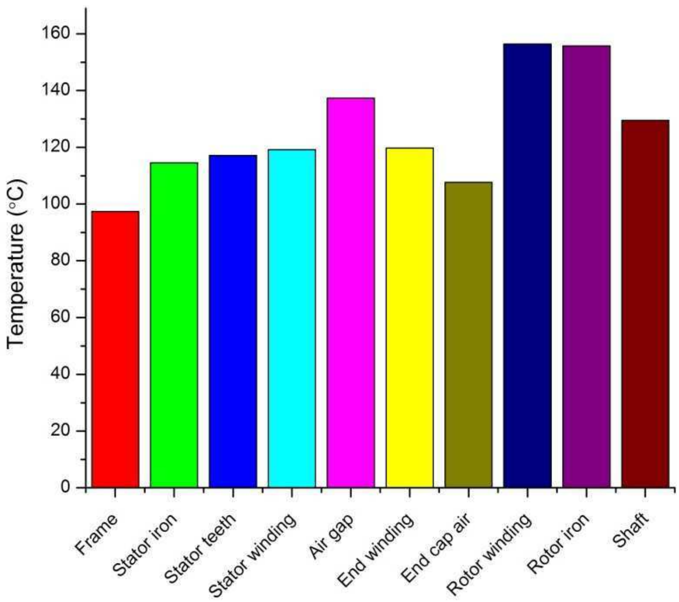

Figure 5.1 Calculated nodal temperatures at the nominal operation point of the 30 kW machine analysis with ambient temperature 40 ℃.

Thermal failure in TEFC induction machine is known to occur in either the stator or rotor windings. The insulation material in the considered motor has thermal class 155. The obtained results show that the temperature of the stator windings does not exceed permitted temperature for this thermal class (see Table 5.2 (Pyrhönen et al. 2008)).

Table 5.2 Thermal classes of insulating materials. Adapted from IEC 60085, IEC 60034-1

Thermal class	Previous designation	Hot spot allowance/ °C	Permitted design temperature rise/K, when the ambient temperature is 40 °C	Permitted average winding temperature determined by resistance measurement/ °C
90	Y	90		
105	A	105	60	
120	E	120	75	
130	B	130	80	120
155	F	155	100	140
180	H	180	125	165
200		200		
220		220		
250		250		

5.2 Sensitivity analysis

In order to determine how errors in the model's parameters affect the temperature predictions, a sensitivity analysis was performed. The sensitivity of the developed thermal model to the correctness of the convection coefficients of the different parts of the studied machine was evaluated by changing the convection coefficients by ±50% from the calculated values. As it is shown in Fig. 5.2 that the changing of the convection heat transfer coefficient between frame and ambient has significant effect on the calculated nodal temperatures. When the convection heat transfer coefficient between frame and ambient is increased by 50 % the nodal temperatures are decreased approximately by 16 %. When the coefficient is decreased by 50 % the nodal temperatures are increased by 50 %. The resistance between frame and ambient has a great influence on the temperature, since the heat is dissipated through this resistance. According equation 4.1 the surface area has an effect on the resistance. In order to dissipate the heat to the ambient the housing should have a greater surface area.

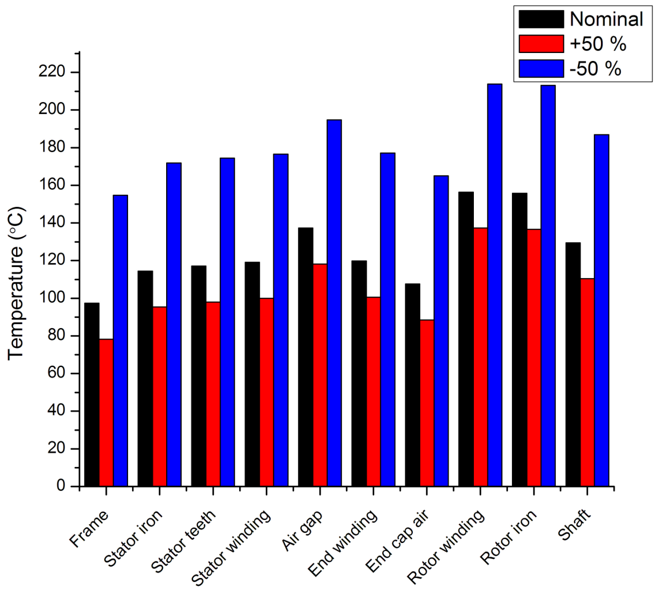

Figure 5.2 Comparison of calculated temperatures with the nominal heat transfer convection coefficient, increased by 50 % and decreased by 50 %.

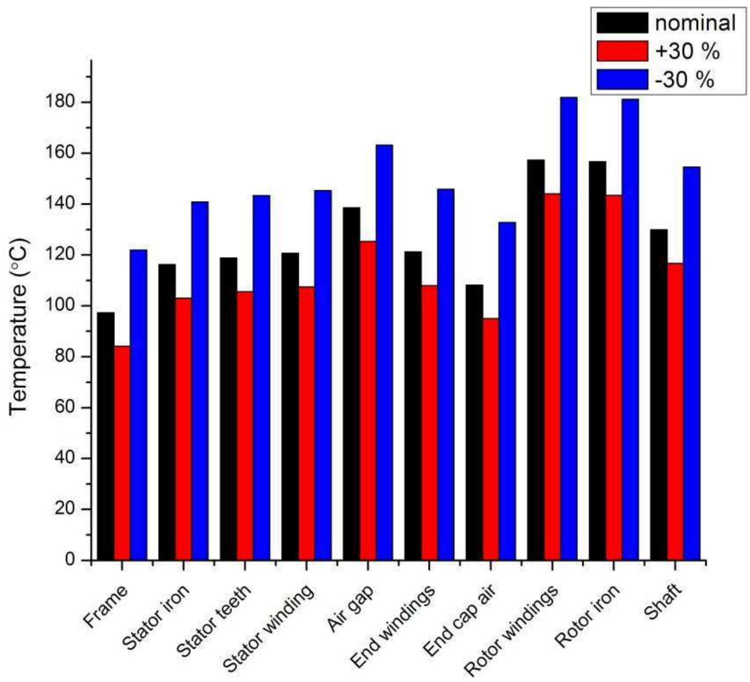

Figure 5.3 Comparison of calculated temperatures with the nominal surface area, increased by 30 % and decreased by 30 %

As shown in Fig. 5.3 when the area is increased by 30 % the calculated temperatures are decreased by approximately 11 %. When the area is decreased the temperatures are increased by 11 %. According the data in Table 3.4 the contact coefficient between the frame and stator core is varied between 350 and 550 W/m^2 K. The temperatures calculated with these values are presented in Fig. 5.4. The biggest influence this coefficient has on the temperature of the stator teeth, stator windings and the stator iron.

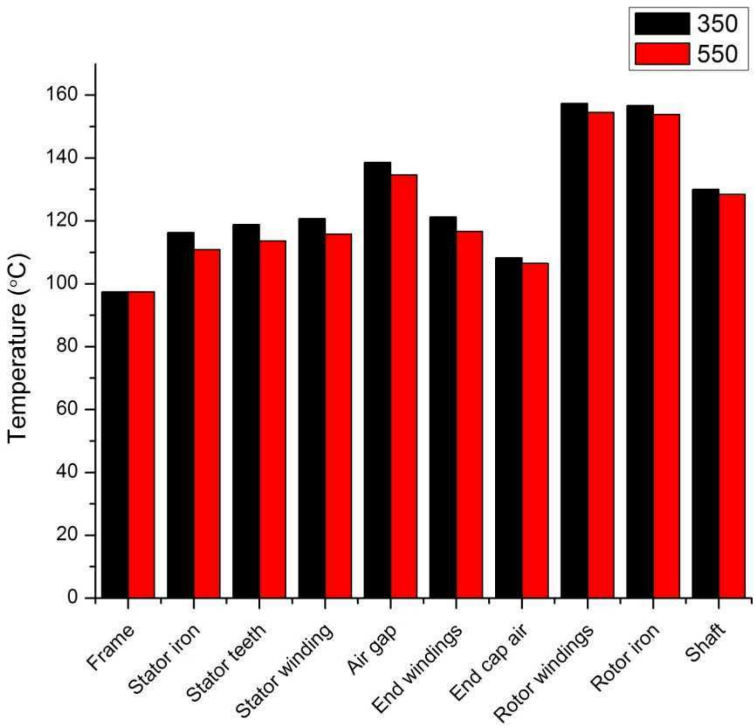

Figure 5.4 Comparison of calculated temperatures with the contact coefficient equals 350 and 550 W/m^2 K

The variation of the convection heat transfer coefficient between stator or rotor and air gap has effect on the temperatures of the rotor windings, the rotor iron, the air gap and the shaft (Fig. 5.5). The convection heat transfer coefficient between stator iron, rotor, end windings or end caps and end cap air has the biggest effect on the temperatures of the rotor windings, the rotor iron and the air gap (Fig. 5.6).

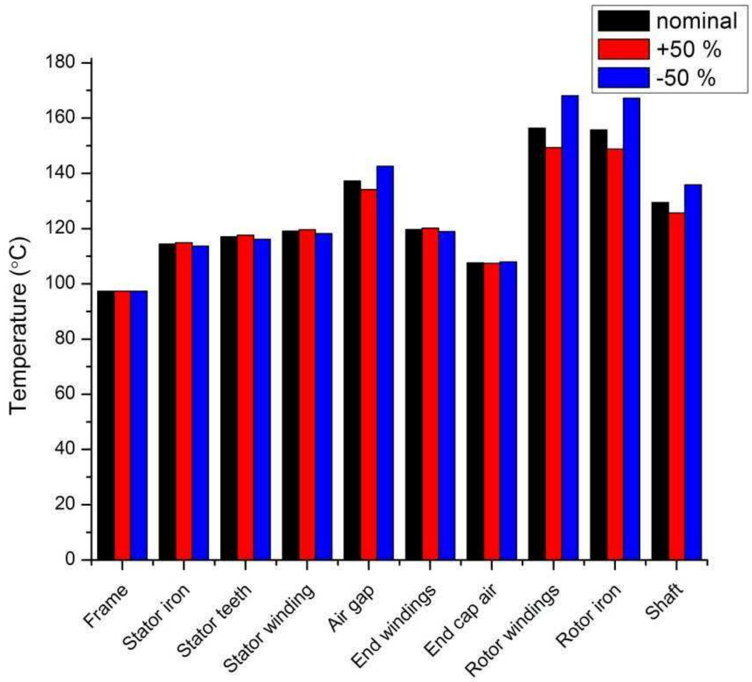

Figure 5.5 Comparison of calculated temperatures with the nominal convection heat transfer coefficient between the stator or rotor and air gap and changed by ±50 %

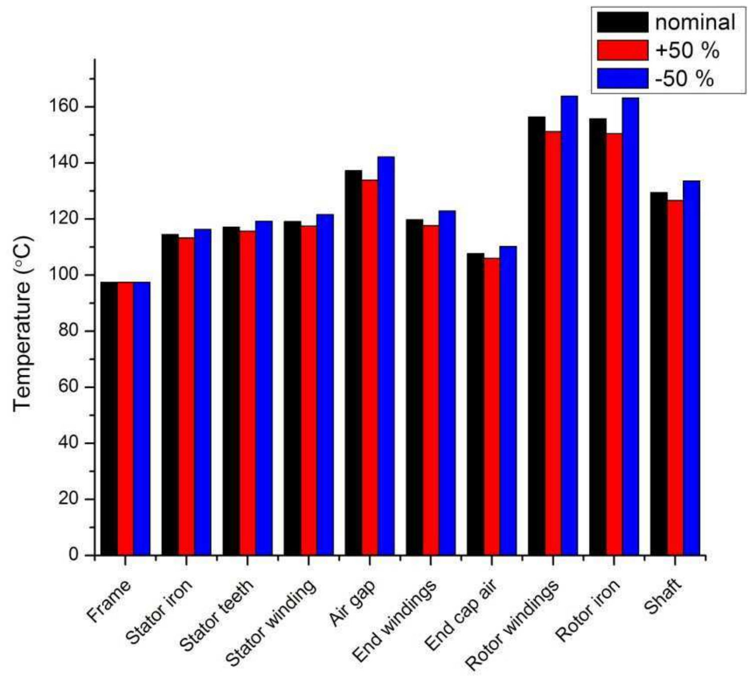

Figure 5.6 Comparison of calculated temperatures with the nominal convection heat transfer coefficient between stator iron, rotor, end windings or end caps and end cap air and changed by ±50 %

The correct estimation of the motor losses is of great importance in the thermal model. The changing of copper losses by ±50 % gives the result introduced in Fig. 5.7.

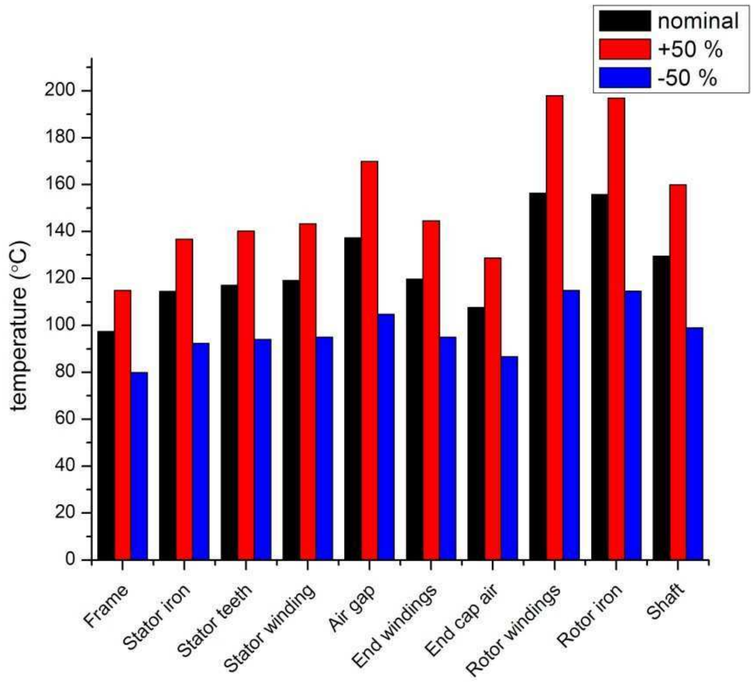

Figure 5.7 Comparison of calculated temperatures with the nominal copper losses, increased by 50 % and decreased by 50 %

The variation of the thermal conductivities and the dimensions has only a minor effect on the temperature prediction.

6 CONCLUSIONS

In the course of the thesis a lumped-parameter model is developed for the thermal analysis of TEFC squirrel cage induction machines. This model is known to be an effective analytical method of estimating the steady-state temperatures in the machine. The geometry of the machine is subdivided into the 10 components presented the most essential machine parts. The distribution of heat sources in the different parts of the machine is considered. The losses are calculated analytically. All the major heat removal mechanisms (conduction, convection, radiation) are modelled in terms of the thermal resistances. The thermal resistances are derived from entirely dimensional information, the thermal properties of materials and constant heat transfer coefficients. The thermal network comprises 37 thermal resistances and 4 heat generators as heat sources of the model.

The benefit of an analytical model when compared to numerical methods is the lower computation time. The model can be easily applied for most TEFC machines. But the accuracy of the analytical model is limited due to several simplifications. The sensitivity analysis is performed to know which parameters are the most sensitive ones so that they can be determined as accurately as possible. From the sensitivity analysis it is known that there are only few resistances that significantly affect the temperatures, while the majority has only a minor effect.

There are a few issues for the future development. The model can be extended to provide a transient solution by including thermal storages as additional heat transfer routes in dynamical states at nodes. For the machine with high power density the model should be modified in order to take into account the heating of the cooling fluid. The assumptions and simplifications made in the model can be validated by comparing the results with measurement results. The results of the analytical method can also be compared with the results of a numerical method based analysis, for example with a FEM-based method.

REFERENCES

Becker, K. M. and Kaye. The influence of a radial temperature gradient on the instability of fluid flow in an annulus with an inner rotating cylinder. *J. Heat Transfer, 84,* 106-110. J. 1962

Boglietti, A., Cavagnino, A., Lazzari, M. and Pastorelli, M. “A simplified thermal model for variable-speed self-cooled industrial induction motor.” *IEEE Trans. Ind. Appl.*, vol. 39, no. 4, pp. 945–952. Jul./Aug. 2003.

Boys, J. T. and Miles, M. J. “Empirical thermal model for inverter-driven cage induction machines.” *Proc. Inst. Elect. Eng.—Elect. Power Appl.*, vol. 141, no. 6, pp. 360–372. Nov. 1995.

Champenois, G., Roye, D. and Zhu, D. S. “Electrical and thermal performance predictions in inverter-fed squirrel-cage induction motor drives.” *Elect. Mach. Power Syst.*, vol. 22, no. 3, pp. 335–370. 1994.

Churchill, S. W., Chu, H. H. S. International Journal of Heat and Mass Transfer, vol. 18, p. 1049. 1972.

Dorrrell, D. G., Staton, D. A., Hahout, J., Hawkins, D. and McGilp, M. I., Apr. “Linked electromagnetic and thermalmodelling of a permanent magnet motor.” in *Proc. IEEE PEMD*, Dublin, Ireland, pp. 536–540. 2006.

Driesen, J. “Coupled electromagnetic–thermal problems in electrical energy transducers.” Ph.D. dissertation, Katholieke Universiteit Leuven, Leuven, Belgium. 2000.

Gao, Z., Habetler, T. G., Harley, R. G. and Colby, R. S. “A sensorless rotor temperature estimator for induction machines based on a current harmonic spectral estimation scheme.” *IEEE Trans. Ind. Electron.*, vol. 55, no. 1, pp. 407–416. Jan. 2008.

Gazley, C. 'Heat Transfer Characteristics of rotating and axial flow between concentric cylinders', Trans ASME, pp.79-89. Jan 1958.

General Electric. ‘Heat transfer and fluid flow data book’. 1969.

Holman, J. P. *Heat Transfer*. New York: McGraw-Hill. 1997.

Kylander, G. “Temperature simulation of a 15 kW induction machine operated at variable speed.” in *Proc. ICEM*, Manchester, U.K., Sep. 15–17, pp. 943–947. 1992.

Kylander, G. “Thermal modeling of small cage-induction motors.” Ph.D. dissertation, Chalmers Univ. Technol., Gothenburg, Sweden. 1995.

Luke, G.F. The cooling of electric machines’, *Trans. AIEE,*45, pp. 1278-1288. 1923.

Mellor, P., Roberts, D. and Turner, D. “Lumped parameter thermal model for electrical machines of TEFC design.” Proc. Elect. Eng., vol. 138,no. 5, pp. 205-218. Sep. 1991.

Mezani, S., Talorabet, N. and Laporte, B. “A combined electromagnetic and thermal analysis of induction motors.” *IEEE Trans. Magn.*, vol. 41, no. 5, pp. 1572–1575. May 2005.

Modest, M. F. *Radiative Heat Transfer*. New York: Academic. 2003.

Mugglestone, J., Pickering, S. J. and Lampard, D. “Effect of geometric changes on the flow and heat transfer in the end region of a TEFC induction motor.” in *Proc. 9th IEEE Int. Conf. Elect. Mach. Drives*, Canterbury, U.K., pp. 40–44. Sep. 1999.

Nelson, J. J., Venkataramanan, G. and El-Refaie, A. M. “Fast thermal profiling of power semiconductor devices using Fourier techniques.” *IEEE Trans. Ind. Electron.*, vol. 53, no. 2, pp. 521–529. Apr. 2006.

Nerg, J., Rilla, M. and Pyrhönen, J. ‘Thermal analysis of radial-flux electrical machines with a high power density,’ *IEEE Trans. Ind. Electron.*, vol. 55, no. 10, pp. 3543–3554. Oct. 2008.

Rajagopal, M. S., Seetharamu, K. N. and Aswathnarayanna, P. A. “Transient thermal analysis of induction motors.” IEEE Trans. Energy Convers., vol. 13, no. 1, pp. 62-69. Mar. 1998.

Rea, S. N. and West, S. E. ‘Thermal radiation from finned heat sinks’, *IEEE Trans. Parts, Hybrids, Packag.*, vol. PHP-12, no. 2, pp. 115–117. Jun. 1976.

Roberts, D. ‘The application of an induction motor thermal model to motor protection and other functions’. PhD thesis, University of Liverpool. 1986

Pyrhönen, J., Jokinen, T. and Hrabovcova, V. *Design of Rotating Electrical Machines*. Chichester: John Wiley & Sons, Ltd. 2008.

Saari, J. “Thermal modelling of high-speed induction machines.” M.S. thesis, Acta Polytechnica Scandinavica, Espoo, Finland. 1995.

Saari, J. “Thermal analysis of high-speed induction machines.” Ph.D. dissertation, Helsinki Univ. Technol., Espoo, Finland. 1998.

(Scribd) Internet source: http://www.scribd.com/ Date of reference 23.4.2010

Sen, P. K., Landa, H. A. Derating of Induction Motors due to waveform distortion, IEEE Transactions on Industry Applications, Vol. 26, No. 6, p. 1102-1107. 1990.

Staton, D. A. “Thermal computer aided design—Advancing the revolution in compact motors.” in *Proc. IEEE IEMDC*, Boston, MA, pp. 858–863. Jun. 2001.

Staton, D. A., Pickering, S. J. and Lampard, D. “Recent advancement in the thermal design of electric motors.” in *Proc. SMMA—Fall Tech. Conf.*, Durham, NC, Oct. 3–5. 2001.

Staton, D. A., Boglietti, A. and Cavagnino, A. “Solving the More Difficult Aspects of Electric Motor Thermal Analysis in Small and Medium Size Industrial Induction Motors.” IEEE Trans. Energy Convers., vol. 20, no. 3, pp. 620-628. Sep. 2005.

Steven, R. E. Electrical Machines and Power Electronics. New York: Van Nostrand-Reinhold. 1983.

Taylor, G.I. 'Distribution of Velocity and Temperature between Concentric Cylinders', Proc Roy Soc, 159, PtA, pp 546-578. 1935.

Trigeol, J. F., Bertin, Y. and Lagonotte, P. “Thermal modeling of an induction machine through the association of two numerical approaches.” *IEEE Trans. Energy Convers.*, vol. 21, no. 2, pp. 314–323. Jun. 2006.

Vong, P. K. and Rodger, D. “Coupled electromagnetic–thermal modeling of electrical machines.” *IEEE Trans.Magn.*, vol. 39, no. 3, pp. 1614–1617. May 2003.

APPENDICES

APPEDNDIX 1

The thermal resistances calculation

Motor dimensions

$l' = 0.2066$ m — Stator length

$r_1 := \frac{D_{se}}{2}$ $\quad r_1 = 0.169$ m — Stator outer radius

$r_2 := \frac{D_{ys} - h_{ys}}{2}$ $\quad r_2 = 0.1351$ m — Tooth outer radius

$\tau_u := b_{1s} + b_{ds}$ $\quad \tau_u = 0.0106$ m — Tooth pitch

$n := Q_s$ $\quad n = 48$ — Number of slots

$r_3 := \frac{D_s}{2}$ $\quad r_3 = 0.1075$ m — Tooth inner radius

$r_4 := \sqrt{\frac{S_{slot}}{\pi}}$ $\quad r_4 = 8.5718 \times 10^{-3}$ m — Equivalent winding radius

$d_i := 0.0005$ m — Insulation thickness

$S_c := S_{Cus}$ $\quad S_c = 1.9066 \times 10^{-4}$ m^2 — Copper cross section in slots

$D_r = 0.2134$ m — Rotor outer diameter

$r_5 := \frac{D_r}{2}$ $\quad r_5 = 0.1067$ m — Rotor outer radius

$r_t := \frac{r_2 + r_3}{2}$ $\quad r_t = 0.1213$ m $\quad$ Endwinding toriod radius

$r_6 := \sqrt{\frac{S_{Cus}}{\pi}} \cdot 3.5$ $\quad r_6 = 0.0273$ m $\quad$ Endwinding cross section radiu

$l_0 := l_{ew}$ $\quad l_0 = 0.025$ m $\quad$ Slot winding overhang

$r_7 := \frac{D_r - 2(h_{1r} + h_{2r} + h_{4r})}{2}$ $\quad r_7 = 0.0889$ m $\quad$ End-disk inner radius

$r_8 := \frac{D_{ring}}{2}$ $\quad r_8 = 0.0975$ m $\quad$ Equivalent rotor winding radiu

$l_e := \frac{S_{ring}}{h_{2r} + h_{4r}}$ $\quad l_e = 0.0365$ m $\quad$ End-disk width

$r_9 := \frac{D_{yr} - h_{yr}}{2}$ $\quad r_9 = 0.0551$ m $\quad$ Shaft radius

$l_m := 0.15$ m $\quad$ Distance of bearing centre to rotor mean

$l_b := 0.025$ m $\quad$ Bearing housing width

$r_{frame} := r_1 + 0.02$ m $\quad$ Frame radius

$D_{frame} := r_{frame} \cdot 2$ m $\quad$ Frame diameter

$l_{endcap} := l_m + \frac{l_b}{2} - \frac{l'}{6}$ $\quad l_{endcap} = 0.1281$ m $\quad$ Endcap length

$l_{frame} := \left(l_m + \frac{l_b}{2}\right) + \frac{l'}{3}$ $\quad l_{frame} = 0.2314$ m $\quad$ Frame length

$S_1 := (2 \cdot \pi \cdot r_{frame} \cdot l_{endcap}) + (\pi \cdot r_{frame}^2)$ $\quad$ Contact area of endcap

$$S_2 := \pi\cdot\left(r_1^{\,2} - r_2^{\,2}\right)$$ Contact area of stator iron

$$S_3 := \pi\cdot\left(r_2^{\,2} - r_3^{\,2}\right) - S_{slot}\cdot n$$ Contact area of stator teeth

$$S_4 := 2\pi\cdot r_6\cdot\left(2\cdot\pi\cdot r_t\right)$$ Contact area of endwinding

$$S_5 := \pi\cdot\left[r_5^{\,2} - \left[\frac{D_r - 2\left(h_{1r} + h_{2r} + h_{4r}\right)}{2}\right]^2\right]$$ Contct area of rotor end-disk

$$S_6 := \pi\cdot\left[\left[\frac{D_r - 2\left(h_{1r} + h_{2r} + h_{4r}\right)}{2}\right]^2 - \left(\frac{D_{yr} - h_{yr}}{2}\right)^2\right]$$ Contact area of rotor iron

$$S_{frame} := \pi\cdot r_{frame}^{\,2} + 2\cdot\pi\cdot r_{frame}\cdot l_{frame}$$ Surface area of the frame

Heat transfer coefficients

$\lambda_{cont} := 400$ W/m²·K Frame-core contact coefficient

$s := 0.97$ Lamination stacking factor

$F_r := 2.5$ Radial conductivity factor

$\omega := 1.5$ Hotspot to mean temperature ratio

Thermal conductivities

$\lambda_{la} := 4$ W/m·K Lamination axial conductivity

$\lambda_{lr} := 39$ W/m·K Lamination Iron conductivity

$\lambda_s := 40$ W/m·K Shaft steel conductivity

$\lambda_c := 400$ W/m·K Copper conductivity

$\lambda_i := 0.8$ W/m·K Slot linear conductivity

$\lambda_v := 0.8$ W/m·K Varnish conductivity

$\lambda_a := 237$ W/m·K Aluminium conductivity

Convection coefficients

Frame to ambient film coefficient

$\lambda_{air} := 0.026$ W/(m·K) theraml conductivity of the air

$\beta := 1 \div 313$ 1/K the coefficient of thermal expansion

$g := 9.81$ m/s^2 the gravitational constant

$\Delta T_1 := 40$ K the temperature difference between the surface and the f

$\nu := 16 \cdot 10^{-6}$ m^2/s the fluid kinematic viscosity

$Pr := 0.708$ Prandtl number

$$Ra := \frac{g \cdot \beta \cdot \Delta T_1 \cdot D_{frame}^{3}}{\nu^2} \qquad Ra = 2.6443 \times 10^8$$ Rayleigh number

convection heat transfer coefficient between frame and ambient

$$\lambda_1 := \frac{\lambda_{air}}{D_{frame}} \cdot \left[\frac{1.36 \cdot 0.518 \cdot Ra^{\frac{1}{6}}}{\left[1 + \left(\frac{0.559}{Pr} \right)^{\frac{9}{16}} \right]^{\frac{8}{27}}} \right]^2 \qquad \lambda_1 = 15.0952$$ W/m^2·K

Air-gap film coefficients

$\mu := 1.8673 \times 10^{-5}$ kg/(m·s) the dinamic viscosity of the air

$\rho_{air} := 1.146$ kg/m^3 density of the air

$n_n := 1474$ 1 /m speed of the rotor

$$v := \frac{(2 \cdot \pi r_5) n_n}{60}$$

The Reynold number is

$$Re := \rho_{air} \cdot v \cdot \frac{\delta}{\mu} \qquad Re = 808.6322$$

Taylor number is

$$Ta := Re^2 \cdot \frac{2\delta}{D_r} \qquad Ta = 4.9026 \times 10^3$$

$$F_g := \frac{\left[\pi^4 \cdot \left(\frac{2r_5 - 2.304\delta}{2r_5 - \delta}\right)\right]}{1697\left[0.0056 + 0.0571\left(\frac{2r_5 - 2.304\delta}{2r_5 - \delta}\right)^2\right]\left(1 - \frac{\delta}{2r_5}\right)} \qquad F_g = 0.9226$$

$$Tam := \frac{Ta}{F_g} \qquad Tam = 5.3137 \times 10^3$$

$$Nu_r := 0.128 \cdot Tam^{0.367} \qquad Nu_r = 2.9815$$

$$Nu_s := 2$$

$\lambda_{2r} := Nu_r \cdot \frac{\lambda_{air}}{\delta}$ $\lambda_{2r} = 96.8975$ W/m^2·K Rotating airgap film coefficient

$\lambda_{2s} := Nu_s \cdot \frac{\lambda_{air}}{\delta}$ $\lambda_{2s} = 65$ W/m^2·K Stationary airgap film coefficien

Endcap film coefficients

$\lambda_{3s} := 15.5$ W/m^2·K stationary endcap film coefficient

$\eta_f := 0.5$ because of the lack of available information on the radial air velocity, a rather arbitrary value of 50% was assumed for the fan efficiency

$\omega_r := 308.55$ 1/s rotor angular velocity

$\nu_f := r_8 \cdot \omega_r \cdot \eta_f$ the cooling air velocity

$$\lambda_{3r} := 15.5 \cdot \left(0.29 \cdot \nu_f + 1\right)$$

$\lambda_{3r} = 83.0951$ W/m^2·K rotating endcap film coefficient

Thermal resistances

$$R1 := \frac{1}{2\lambda_1 \cdot 1.51 S_{frame}}$$

$$R2 := \frac{1}{\pi \cdot \lambda_{cont} \cdot l' \cdot r_1}$$

$$R3 := \frac{l'}{6 \cdot \pi \cdot \lambda_{la} \cdot \left[r_1^{\,2} - \left(r_2\right)^2\right]}$$

$$R4 := \frac{-1\left[\left(r_1\right)^2 + \left(r_2\right)^2 - \dfrac{4 \cdot \left(r_1\right)^2 \cdot \left(r_2\right)^2 \cdot ln\left(\dfrac{r_1}{r_2}\right)}{\left(r_1\right)^2 - \left(r_2\right)^2}\right]}{4 \cdot \pi \cdot \lambda_{lr} \cdot l' \cdot s \cdot \left[\left(r_1\right)^2 - \left(r_2\right)^2\right]}$$

$$R5 := \frac{1 - \dfrac{2 \cdot \left(r_2\right)^2 \cdot ln\left(\dfrac{r_1}{r_2}\right)}{\left(r_1\right)^2 - \left(r_2\right)^2}}{2 \cdot \pi \cdot \lambda_{lr} \cdot l' \cdot s}$$

$$R6 := \frac{\left[\frac{2\cdot (r_1)^2 \cdot ln\left(\frac{r_1}{r_2}\right)}{(r_1)^2 - (r_2)^2}\right] - 1}{2\cdot \pi \cdot \lambda_{lr} \cdot l' \cdot s}$$

$$R7 := \frac{l' \cdot \tau_u}{6\cdot \pi \cdot \lambda_{la} \cdot b_{ds} \cdot \left[(r_2)^2 - (r_3)^2\right]}$$

$$R8 := \frac{\pi \cdot b_{ds} \cdot \left[(r_2)^2 - (r_3)^2\right]}{\lambda_{lr} \cdot l' \cdot s \cdot \tau_u \cdot (r_2 - r_3)^2 \cdot n^2}$$

$$R9 := \frac{-\tau_u \cdot \left[(r_2)^2 + (r_3)^2 - \frac{4\cdot (r_2)^2 \cdot (r_3)^2 \cdot ln\left(\frac{r_2}{r_3}\right)}{(r_2)^2 - (r_3)^2}\right]}{4\cdot \pi \cdot \lambda_{lr} \cdot l' \cdot s \cdot b_{ds} \cdot \left[(r_2)^2 - (r_3)^2\right]}$$

$$R10 := \frac{\tau_u \cdot \left[1 - \frac{2\cdot (r_3)^2 \cdot ln\left(\frac{r_2}{r_3}\right)}{(r_2)^2 - (r_3)^2}\right]}{2\cdot \pi \cdot \lambda_{lr} \cdot l' \cdot s \cdot b_{ds}}$$

$$R11 := \frac{\tau_u \cdot \left[\left[\frac{2\cdot (r_2)^2 \cdot ln\left(\frac{r_2}{r_3}\right)}{(r_2)^2 - (r_3)^2}\right] - 1\right]}{2\cdot \pi \cdot \lambda_{lr} \cdot l' \cdot s \cdot b_{ds}}$$

$$R12 := \frac{2\cdot d_i}{\pi \cdot \lambda_i \cdot l' \cdot r_4 \cdot n} + \frac{1}{2\cdot \pi \cdot \lambda_v \cdot l' \cdot F_r \cdot n}$$

$$R13 := \frac{l'}{6 \cdot \pi \cdot \lambda_c \cdot S_c \cdot n}$$

$$R14 := \frac{4 \cdot d_i}{\pi \cdot \lambda_i \cdot l' \cdot r_4 \cdot n} + \frac{1}{\pi \cdot \lambda_\nu \, l' \cdot F_r \cdot n}$$

$$R15 := \frac{1}{\pi \cdot \lambda_\nu \, l' \cdot F_r \cdot n}$$

$$R16 := \frac{\tau_u}{b_{ds} \cdot \pi \cdot r_3 \cdot l' \cdot \lambda_{2r}}$$

$$R17 := \frac{\tau_u}{\left(\tau_u - b_{ds}\right) \cdot \pi \cdot r_3 \cdot l' \cdot \lambda_{2r}}$$

$$R18 := \frac{1}{\pi \cdot r_5 \cdot l' \cdot \lambda_{2r}}$$

$$R19 := \frac{l_0 \cdot \omega}{n \cdot S_c \cdot \lambda_c}$$

$$R20 := \frac{\omega}{16 \cdot \pi^2 \cdot r_t \cdot F_r \cdot \lambda_\nu}$$

$$R21 := \frac{\omega \cdot \left(r_6\right)^2}{8 \cdot \pi \cdot \left(r_4\right)^2 \cdot l_0 \cdot F_r \cdot \lambda_\nu \, n}$$

$$R22 := \frac{1}{S_1 \cdot \lambda_{3r}}$$

$$R23 := \frac{1}{S_2 \cdot \lambda_{3r}}$$

$$R24 := \frac{1}{S_3 \cdot \lambda_{3r}}$$

$$R25 := \frac{1}{1.5 S_4 \cdot \lambda_{3r}}$$

$$R26 := \frac{1}{S_5 \cdot \lambda_{3r}}$$

$$R27 := \frac{1}{S_6 \cdot \lambda_{3r}}$$

$$R28 := \frac{l'}{6 \cdot \pi \cdot \lambda_a \cdot \left[\left(r_5\right)^2 - \left(r_8\right)^2 \right]} + \frac{l_e}{\pi \cdot \lambda_a \cdot \left[\left(r_5\right)^2 - \left(r_7\right)^2 \right]}$$

$$R29 := \frac{-1}{4 \cdot \pi \cdot \lambda_a \cdot l' \cdot \left[\left(r_5\right)^2 - \left(r_8\right)^2 \right]} \cdot \left[\left(r_5\right)^2 + \left(r_8\right)^2 - \frac{4 \cdot \left(r_5\right)^2 \cdot \left(r_8\right)^2 \cdot ln\left(\frac{r_5}{r_8}\right)}{\left(r_5\right)^2 - \left(r_8\right)^2} \right]$$

$$R30 := \frac{1}{2 \cdot \pi \cdot \lambda_a \cdot l'} \cdot \left[1 - \frac{2 \cdot \left(r_8\right)^2 \cdot ln\left(\frac{r_5}{r_8}\right)}{\left(r_5\right)^2 - \left(r_8\right)^2} \right]$$

$$R31 := \frac{1}{2 \cdot \pi \cdot \lambda_a \cdot l'} \cdot \left[\frac{2 \cdot \left(r_5\right)^2 \cdot ln\left(\frac{r_5}{r_8}\right)}{\left(r_5\right)^2 - \left(r_8\right)^2} - 1 \right]$$

$$R32 := \frac{l'}{6 \cdot \pi \cdot \lambda_{la} \cdot \left[\left(r_8\right)^2 - \left(r_9\right)^2 \right]}$$

$$R33 := \frac{-1}{4\cdot\pi\cdot\lambda_{lr}\cdot l\acute{}\cdot s\cdot\left[\left(r_8\right)^2-\left(r_9\right)^2\right]}\cdot\left[\left(r_8\right)^2+\left(r_9\right)^2-\frac{4\cdot\left(r_8\right)^2\cdot\left(r_9\right)^2\cdot ln\left(\frac{r_8}{r_9}\right)}{\left(r_8\right)^2-\left(r_9\right)^2}\right]$$

$$R34 := \frac{\left(r_8\right)^2-\left(r_9\right)^2}{2\cdot\pi\cdot\lambda_{lr}\cdot l\acute{}\cdot s\cdot\left[\left(r_8\right)^2-\left(r_9\right)^2\right]}\cdot\left[1-\frac{2\cdot\left(r_9\right)^2\cdot ln\left(\frac{r_8}{r_9}\right)}{\left(r_8\right)^2-\left(r_9\right)^2}\right]$$

$$R35 := \frac{\left(r_8\right)^2-\left(r_9\right)^2}{2\cdot\pi\cdot\lambda_{lr}\cdot l\acute{}\cdot s\cdot\left[\left(r_8\right)^2-\left(r_9\right)^2\right]}\cdot\left[\frac{2\cdot\left(r_8\right)^2\cdot ln\left(\frac{r_8}{r_9}\right)}{\left(r_8\right)^2-\left(r_9\right)^2}-1\right]$$

$$R36 := \frac{1}{2\cdot\pi\cdot\lambda_s\cdot l\acute{}}+\frac{l_m}{2\cdot\pi\cdot\lambda_s\cdot\left(r_9\right)^2}$$

$$R37 := \frac{1}{4\cdot\pi\cdot\lambda_s\cdot l_b}+\frac{l_m}{2\cdot\pi\cdot\lambda_s\cdot\left(r_9\right)^2}$$

Thermal conductances

$$g_{12} := \frac{1}{R2+R4+R5}$$

$$g_{17} := \frac{1}{R22}$$

$$g_{110} := \frac{1}{R37}$$

$$g_{11} := g_{12}+g_{110}+g_{17}+\frac{1}{R1}$$

$$g_{23} := \frac{1}{R4+R6+R9+R10}$$

$$g_{24} := \frac{1}{R14 + R6 + R4}$$

$$g_{25} := \frac{1}{R4 + R6 + R10 + R11 + R16}$$

$$g_{27} := \frac{1}{R3 + R23}$$

$$g_{22} := g_{12} + g_{23} + g_{27} + g_{24}$$

$$g_{34} := \frac{1}{R8 + R12}$$

$$g_{35} := \frac{1}{R9 + R11 + R16}$$

$$g_{37} := \frac{1}{R7 + R24}$$

$$g_{33} := g_{23} + g_{34} + g_{37} + g_{35}$$

$$g_{45} := \frac{1}{R15 + R17}$$

$$g_{46} := \frac{1}{R13 + R19}$$

$$g_{44} := g_{24} + g_{34} + g_{45} + g_{46}$$

$$g_{58} := \frac{1}{R18 + R29 + R30}$$

$$g_{55} := g_{35} + g_{45} + g_{58}$$

$$g_{67} := \frac{1}{\left(\frac{R20 \cdot R21}{R20 + R21}\right) + R25}$$

$$g_{66} := g_{46} + g_{67}$$

$$g_{78} := \frac{1}{R26 + R28}$$

$$g_{79} := \frac{1}{R32 + R27}$$

$$g_{77} := g_{17} + g_{27} + g_{37} + g_{67} + g_{78} + g_{79}$$

$$g_{89} := \frac{1}{R29 + R31 + R33 + R34}$$

$$g_{88} := g_{58} + g_{78} + g_{89}$$

$$g_{910} := \frac{1}{R33 + R35 + R36}$$

$$g_{99} := g_{89} + g_{910} + g_{79}$$

$$g_{1010} := g_{910} + g_{110}$$

$$G := \begin{pmatrix} g_{11} & -g_{12} & 0 & 0 & 0 & 0 & -g_{17} & 0 & 0 & -g_{110} \\ -g_{12} & g_{22} & -g_{23} & -g_{24} & 0 & 0 & -g_{27} & 0 & 0 & 0 \\ 0 & -g_{23} & g_{33} & -g_{34} & -g_{35} & 0 & -g_{37} & 0 & 0 & 0 \\ 0 & -g_{24} & -g_{34} & g_{44} & -g_{45} & -g_{46} & 0 & 0 & 0 & 0 \\ 0 & 0 & -g_{35} & -g_{45} & g_{55} & 0 & 0 & -g_{58} & 0 & 0 \\ 0 & 0 & 0 & -g_{46} & 0 & g_{66} & -g_{67} & 0 & 0 & 0 \\ -g_{17} & -g_{27} & -g_{37} & 0 & 0 & -g_{67} & g_{77} & -g_{78} & -g_{79} & 0 \\ 0 & 0 & 0 & 0 & -g_{58} & 0 & -g_{78} & g_{88} & -g_{89} & 0 \\ 0 & 0 & 0 & 0 & 0 & 0 & -g_{79} & -g_{89} & g_{99} & -g_{910} \\ -g_{110} & 0 & 0 & 0 & 0 & 0 & 0 & 0 & -g_{910} & g_{1010} \end{pmatrix}$$

$$P := \begin{bmatrix} 0 \\ \dfrac{P_{Feys}}{2} \\ \dfrac{P_{Feds} + 0.3 \cdot P_{ad_{1474}}}{2} \\ \dfrac{\left(P_{Cus_{1474}}\right) \cdot 0.48 + 0.4 \cdot P_{ad_{1474}}}{2} \\ 0 \\ \dfrac{\left(P_{Cus_{1474}}\right) \cdot 0.52}{2} \\ 0 \\ \dfrac{\left(P_{Cur_{1474}}\right)}{2} \\ \dfrac{0.3 \cdot P_{ad_{1474}}}{2} \\ 0 \end{bmatrix}$$

$$\Delta T := G^{-1} \cdot P \qquad \Delta T = \begin{pmatrix} 57.3947 \\ 74.5071 \\ 77.1121 \\ 79.1349 \\ 97.3152 \\ 79.7574 \\ 67.6558 \\ 116.4214 \\ 115.7548 \\ 89.4906 \end{pmatrix}$$

temperature rise vector

$$T_{ambient} := \begin{pmatrix} 40 \\ 40 \\ 40 \\ 40 \\ 40 \\ 40 \\ 40 \\ 40 \\ 40 \\ 40 \end{pmatrix} \ {}^\circ C \qquad T := \Delta T + T_{ambient}$$

$$T = \begin{pmatrix} 97.3947 \\ 114.5071 \\ 117.1121 \\ 119.1349 \\ 137.3152 \\ 119.7574 \\ 107.6558 \\ 156.4214 \\ 155.7548 \\ 129.4906 \end{pmatrix} \ {}^\circ C$$